

7-Phenoxy-Substituted 3,4-Dihydro-2*H*-1,2,4-benzothiadiazine 1,1-Dioxides as Positive Allosteric Modulators of α -Amino-3-hydroxy-5-methyl-4-isoxazolepropionic Acid (AMPA) Receptors with Nanomolar Potency

Eric Goffin,^{†,⊥} Thomas Drapier,^{†,⊥} Anja Probst Larsen,[‡] Pierre Geubelle,^{†,§} Christopher P. Ptak,^{||} Saara Laulumaa,[‡] Karoline Rovinskaja,[‡] Julie Gilissen,^{†,§} Pascal de Tullio,[†] Lars Olsen,[‡] Karla Frydenvang,[‡] Bernard Pirotte,[†] Julien Hanson,^{*,†,§} Robert E. Oswald,^{*,||} Jette Sandholm Kastrup,^{*,‡} and Pierre Francotte^{*,†}

[†]Laboratory of Medicinal Chemistry, Center for Interdisciplinary Research on Medicines (CIRM), University of Liège, Quartier Hôpital B36 Av. Hippocrate 15 B-4000 Liège, Belgium

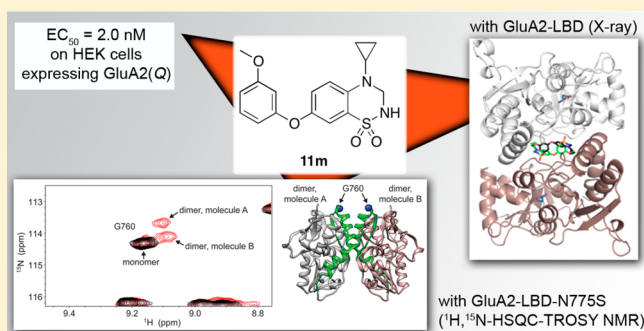
[‡]Biostructural Research, Department of Drug Design and Pharmacology, Faculty of Health and Medical Sciences, University of Copenhagen, DK-2100 Copenhagen, Denmark

[§]Laboratory of Molecular Pharmacology, GIGA-Molecular Biology of Diseases, University of Liège, Liège, Belgium

^{||}Department of Molecular Medicine, Cornell University, Ithaca, New York 14850, United States

Supporting Information

ABSTRACT: We report here the synthesis of 7-phenoxy-substituted 3,4-dihydro-2*H*-1,2,4-benzothiadiazine 1,1-dioxides and their evaluation as AMPA receptor positive allosteric modulators (AMPAPams). The impact of substitution on the phenoxy ring and on the nitrogen atom at the 4-position was examined. At GluA2(Q) expressed in HEK293 cells (calcium flux experiment), the most potent compound was **11m** (4-cyclopropyl-7-(3-methoxyphenoxy)-3,4-dihydro-2*H*-1,2,4-benzothiadiazine 1,1-dioxide, $EC_{50} = 2.0$ nM). The Hill coefficient in the screening and the shape of the dimerization curve in small-angle X-ray scattering (SAXS) experiments using isolated GluA2 ligand-binding domain (GluA2-LBD) are consistent with binding of one molecule of **11m** per dimer interface, contrary to most benzothiadiazine dioxides developed to date. This observation was confirmed by the X-ray structure of **11m** bound to GluA2-LBD and by NMR. This is the first benzothiadiazine dioxide AMPAPam to reach the nanomolar range.



INTRODUCTION

L-Glutamate is well-known as the key excitatory neurotransmitter in the central nervous system, acting through activation of metabotropic receptors (mGluRs, coupled to G-protein) and ionotropic receptors (iGluRs, cation channels).^{1,2} iGluRs are recognized to play a crucial role in the fast excitatory synaptic transmission. They have been classified into three subtypes named after their affinity for nonendogenous ligands: *N*-methyl-D-aspartic acid (NMDA), α -amino-3-hydroxy-5-methyl-4-isoxazolepropionic acid (AMPA), and kainic acid (KA). Among these three subtypes, AMPA receptors (AMPA receptors) have attracted attention, assuming that upregulation of these receptors could lead to cognition enhancement. This idea has been reinforced, taking into account their critical involvement in synaptic plasticity³ and their involvement in the mechanism of action of nootropic drugs.⁴ AMPARs are thus considered as an attractive and appropriate target for the

discovery of cognitive enhancers and a potential therapeutic tool in the management of Alzheimer's disease.⁵ This strategy was even found more promising considering their ability to induce the release of neurotrophic factors in vivo, like BDNF.^{6,7}

While AMPAR agonists are expected to exert excitotoxic effects, AMPAR positive allosteric modulators (so-called "AMPAPams" or AMPAR potentiators) seem more promising, as they are able to fine-tune AMPAR signals through their binding at allosteric sites of the receptors and need the presence of endogenous glutamate to be active.

AMPA receptors are homo/heterotetrameric complexes assembled with GluA1–4 subunits.⁸ Each subunit contains an amino-terminal domain involved in subunit assembly (ATD), a clamshell-shaped domain providing the binding pocket for

Received: September 7, 2017

glutamate (LBD), a transmembrane domain forming the permeation channel for cations (TMD) and a cytoplasmic terminal domain (CTD) associated with processes such as receptor trafficking or regulation.⁹ By their ability to form bridging interactions between LBD dimers, positive allosteric modulators stabilize the receptor in its open state and thus slow deactivation and/or desensitization processes.^{5,10} This may be achieved either with one or two potentiator molecules per dimer, thus with two or four potentiator molecules per AMPAR,¹¹ depending on the occupancy of the A/B/B'/C and C' subsites, which constitute the binding cavity, as previously defined.¹²

Among the different AMPAR potentiators,¹³ 3,4-dihydro-2*H*-1,2,4-benzothiadiazine 1,1-dioxides constitute probably the most investigated chemical class, as exemplified by recent publications (Figure 1).^{14–17}

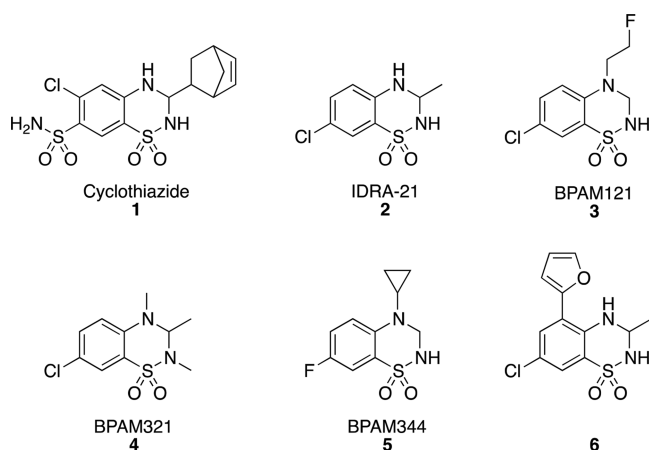


Figure 1. Structures of selected AMPAR potentiators belonging to 3,4-dihydro-2*H*-1,2,4-benzothiadiazine 1,1-dioxides.

Taking advantage of the observation by Cordi et al. that an aryloxy or a heteroaryloxy group at the 7-position of benzothiadiazine dioxides could favorably impact the potentiator activity on AMPARs,¹⁸ the present work focused on the 7-phenoxy-3,4-dihydro-2*H*-1,2,4-benzothiadiazine 1,1-dioxides, exploring the influence of monosubstitution of the phenoxy group introduced at the 7-position. Particular attention was paid to the study of the binding mode of the new compounds

through characterization with SAXS, NMR, and crystallography.

RESULTS AND DISCUSSION

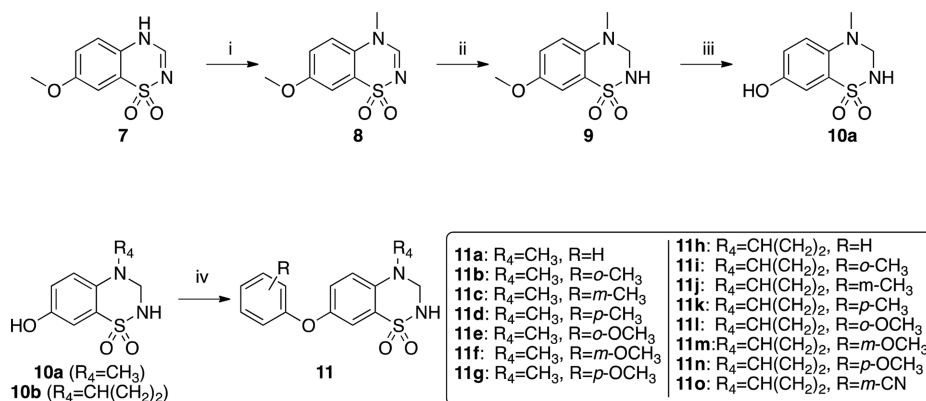
Synthesis. The synthetic pathway used to prepare the 7-phenoxy-substituted 3,4-dihydro-2*H*-1,2,4-benzothiadiazine 1,1-dioxides reported here is illustrated in Scheme 1.

The 7-phenoxy-substituted 3,4-dihydro-2*H*-1,2,4-benzothiadiazine 1,1-dioxides **11** series were prepared from the corresponding intermediates **10** series through a Chan–Lam coupling reaction with the appropriate phenylboronic acid in the presence of copper(II) acetate in dichloromethane. While the intermediate **10b** was obtained as previously described,¹⁶ its 4-methylated analogue **10a** was prepared via an alternate pathway, starting from 7-methoxy-4*H*-1,2,4-benzothiadiazine 1,1-dioxide **7**.¹⁹ After alkylation on the 4-nitrogen atom using methyl iodide in the presence of potassium carbonate in acetonitrile and saturation of the double bond in the 2,3-positions by means of sodium borohydride, conversion of the methoxy at the 7-position into a hydroxyl group was achieved with boron tribromide in dichloromethane giving access to **10a**.

Substituents inserted on the nitrogen atom at the 4-position were selected according to the previously reported structure–activity relationships.^{19,20} While the introduction of the cyclopropyl group in this position was clearly the optimal choice and could thus not be neglected, we decided to also investigate the impact of the insertion of the smallest alkyl radical, namely the methyl group.

Measurement of GluA2-Induced Calcium Flux in HEK293 Cells. The new set of compounds was evaluated in vitro as AMPAR potentiators using a fluorescence-based calcium assay performed on HEK293 cells stably expressing the AMPAR GluA2(Q) in order to evaluate the effect of the compounds on the glutamate-evoked channel opening. For each compound, the pEC₅₀ (negative logarithm of the modulator concentration responsible for 50% of the glutamate maximal effect at 1 mM) value was determined. Results obtained with this newly developed pharmacological assay were in good agreement with results obtained with previously used methods: for example, the mean EC₅₀ values obtained with a previous fluorescence-based calcium measurement assay induced by 300 μM AMPA on primary cultures of neurons from a rat embryonic cortex²¹ for **5**, **11h**, and **11o** were 0.9, 1.0,

Scheme 1. Synthetic Pathway of 7-Phenoxy-Substituted 3,4-Dihydro-2*H*-1,2,4-benzothiadiazine 1,1-Dioxides^a



^aConditions: (i) CH₃I, K₂CO₃, CH₃CN, 60°C, 3 h (81%); (ii) NaBH₄, 2-propanol, rt, 45 min (78%); (iii) BBr₃, CH₂Cl₂, rt, 6 h (76%); (iv) adequately substituted phenylboronic acid, Cu(OAc)₂, molecular sieves, CH₂Cl₂, 40°C, 5 h (13–74%).

Table 1. Potentiating Effects of 7-Phenoxy-Substituted 3,4-Dihydro-2H-1,2,4-benzothiadiazine 1,1-Dioxides on the Calcium Flux Induced by 1 mM Glutamate on HEK293 Cells Stably Expressing the GluA2(Q) Subunit and Hill Coefficient

compound	R ₄	R	pEC ₅₀ ^a	corresponding EC ₅₀ ^b	Hill coefficient ^c
3			4.690 ± 0.013 (3)	20.4	3.0 ± 0.2 (3)
4			4.728 ± 0.012 (3)	18.7	3.0 ± 0.1 (3)
5			6.090 ± 0.004 (3)	0.81	3.5 ± 0.1 (3)
12			4.296 ± 0.008 (3)	50.6	3.0 ± 0.1 (3)
11a	CH ₃	H	5.118 ± 0.019 (3)	7.62	1.4 ± 0.1 (3)
11b	CH ₃	<i>o</i> -CH ₃	<5 (3)	10.0	nd
11c	CH ₃	<i>m</i> -CH ₃	6.408 ± 0.015 (3)	0.39	2.3 ± 0.2 (3)
11d	CH ₃	<i>p</i> -CH ₃	6.020 ± 0.013 (3)	0.95	2.1 ± 0.1 (3)
11e	CH ₃	<i>o</i> -OCH ₃	<5 (3)	>10.0	nd
11f	CH ₃	<i>m</i> -OCH ₃	6.431 ± 0.030 (3)	0.37	2.3 ± 0.4 (3)
11g	CH ₃	<i>p</i> -OCH ₃	5.229 ± 0.035 (3)	5.90	1.7 ± 0.2 (3)
11h	CH(CH ₂) ₂	H	6.147 ± 0.033 (3)	0.71	1.3 ± 0.1 (3)
11i	CH(CH ₂) ₂	<i>o</i> -CH ₃	4.807 ± 0.022 (3)	15.6	1.7 ± 0.1 (3)
11j	CH(CH ₂) ₂	<i>m</i> -CH ₃	7.336 ± 0.027 (3)	0.05	1.1 ± 0.1 (3)
11k	CH(CH ₂) ₂	<i>p</i> -CH ₃	5.496 ± 0.021 (3)	3.19	1.9 ± 0.2 (3)
11l	CH(CH ₂) ₂	<i>o</i> -OCH ₃	4.807 ± 0.018 (3)	15.60	2.3 ± 0.2 (3)
11m	CH(CH ₂) ₂	<i>m</i> -OCH ₃	8.700 ± 0.049 (6)	0.002	1.4 ± 0.2 (6)
11n	CH(CH ₂) ₂	<i>p</i> -OCH ₃	5.740 ± 0.023 (3)	1.82	1.5 ± 0.1 (3)
11o	CH(CH ₂) ₂	<i>m</i> -CN	6.343 ± 0.018 (3)	0.45	1.7 ± 0.1 (3)

^apEC₅₀ = negative logarithm of AMPAR potentiator concentration responsible for 50% of the maximal effect (mean ± SEM (*n*)). ^bMean concentration responsible for 50% of the maximal effect, in μM. ^cMean value ± SEM (*n*).

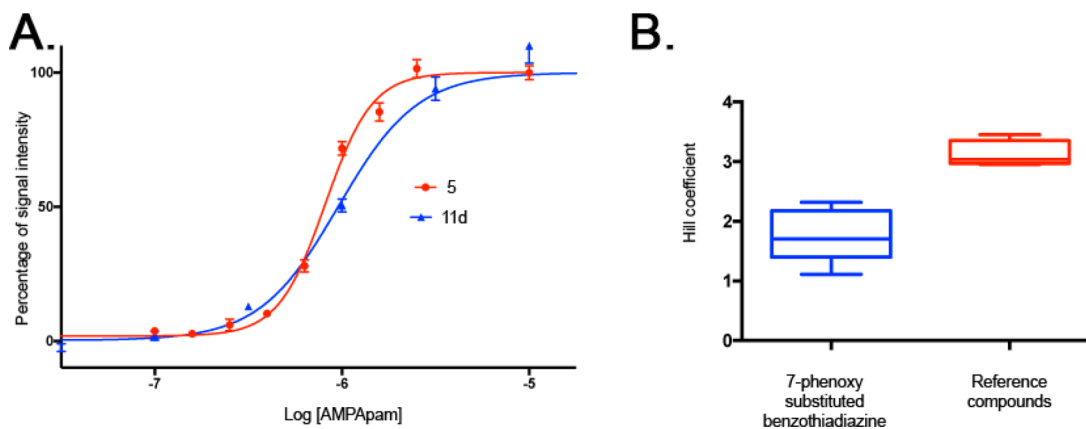


Figure 2. Measurement of GluA2-induced calcium flux in HEK293 cells. (A) Comparison of two activity curves obtained with **11d** and **5**. (B) Comparison of the mean Hill coefficient obtained with the two sets of compounds. The boxes represent the distribution of the values corresponding to the Hill coefficient collected for the two sets; they include a medium line depicting the corresponding mean value for each set and the error bars corresponding to the standard error to the mean.

and 0.4 μM, respectively (*n* = 3). These values are close to those obtained here in heterologously transfected HEK293 cells (EC₅₀ values of 0.81, 0.71, and 0.45 μM, respectively; Table 1).

As previously noticed in other series,²⁰ the introduction of a cyclopropyl group on the nitrogen atom at the 4-position is in most cases more favorable for the activity than introduction of a methyl group (compare **11a** vs **11h**, **11c** vs **11j** or **11f** vs **11m**).

Exploration of the nature of the substitution of the phenoxy moiety was limited but showed that a methyl group seemed to have the same impact on activity as a methoxy group (see **11b**/**11c**/**11d** vs **11e**/**11f**/**11g** and **11i**/**11k** vs **11l**/**11n**). However,

in the 4-cyclopropyl series, the methoxy group surprisingly exerts a drastic change of the activity profile when positioned in the *meta* position of the phenoxy moiety (see **11m**, EC₅₀ = 2.0 nM vs **11j**, EC₅₀ = 46.1 nM). This leads to the most powerful AMPAR potentiator ever designed in our series, namely compound **11m**.

The position of the substitution was found critical for the activity: the rank order of potency was observed following the sequence *meta* > *para* > *ortho*. While the *meta* position for the phenoxy substitution was found to be the best option, the absence of a substitution was found to have a neutral to rather

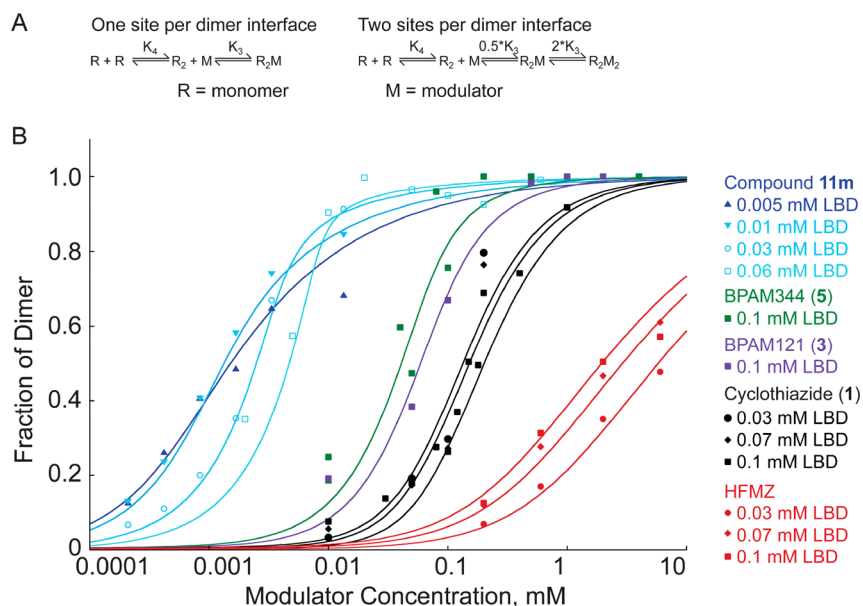


Figure 3. GluA2-LBD-N775S dimerization using SAXS. (A) Dimerization models assuming one site per dimer interface and two sites per dimer interface. K_4 is the dimerization constant and K_3 is the intrinsic binding constant. R is the GluA2-LBD-N775S monomer and M is the free modulator concentration. The model is written to exclude cooperativity of binding. (B) The fraction of dimer observed in the SAXS experiment as a function of the total modulator concentration using various allosteric modulators and different concentrations of GluA2-LBD-N775S. For compound **11m**, the curves are shown in different shades of blue, with the lightest corresponding to the highest concentration of protein. The change in shape of the curve is due to the fact that the protein concentration is in the same range as the modulator concentration, so that it is particularly limiting in the lower ranges of modulator concentration. The lowest protein concentration in this series has a shallow slope similar to that of HFMZ, suggesting one binding site per dimer interface. The steeper slope of the **11m** curve at increasing protein concentrations is caused by the modulator/protein ratio depleting the free modulator. At higher protein concentrations, the dimer fraction becomes particularly limited by the lower range of modulator concentrations.

positive effect comparing to *ortho* or *para* substitution (see **11a** vs **11b/11e/11g** or **11h** vs **11i/11k/11l/11n**). This trend was only contradicted with the methyl group in the *para* substitution (**11a** vs **11d**) in the series bearing a methyl group on the nitrogen atom at the 4-position.

Based on the fact that the *meta* position of the phenoxy group was critical, the preparation of a 7-phenoxy compound substituted with a cyano moiety at the *meta* position was envisaged in order to evaluate the influence of a strong electron-withdrawing group. This compound (**11o**) was found less active than the methyl or methoxy analogues (**11j** and **11m**) and nearly as potent as the unsubstituted phenoxy compound (**11h**). This observation could be explained by the steric interactions of the corresponding group in the *meta* position.

Looking at the slope of the concentration–response sigmoidal curves generated in our new functional assay (see Figure 2A for two representative profiles obtained with **11d** and reference compound **5**, respectively) and keeping in mind the observations previously made with SAXS data,¹¹ the Hill coefficient²² was examined for each curve. This feature of the curve reflects the existence of multiple binding sites in the receptor and enables determination of the binding stoichiometry. This permitted to compare the new compounds **11** and the references **3**, **4**, **5**, and **12** (see Table 1 and Figure 2B). The collected data suggest a distinct stoichiometry for 7-phenoxy compounds **11** compared to reference compounds **3**, **4**, **5**, and **12**; whereas reference compounds bind in two copies on the interface (as previously demonstrated for **5**²³), the compounds **11** bind in one copy. This trend observed here might be explained by a difference in the binding mode within the dimer interface. The figures suggest that the new set of compounds

constitutes a unique subclass in our series of benzothiadiazine dioxides designed to date (Figure 2B). Further investigations (SAXS, crystallography, and NMR) presented hereafter corroborate this observation.

Small-Angle X-ray Scattering (SAXS). The isolated GluA2-LBD-N775S shows only a weak propensity for dimerization, but the ability of allosteric modulators to stabilize dimer formation can be used to assess both affinity and stoichiometry.¹¹ SAXS provides a measure of GluA2-LBD-N775S dimerization because the scattering profile of the GluA2-LBD-N775S changes markedly upon dimerization allowing the contributions of monomer and dimer curves to be determined by standard fitting routines (OLIGOMER).²⁴ The fraction of dimer at each modulator condition is then modeled using the schemes shown in Figure 3A. All curves were fit simultaneously, with a common K_4 value (dimerization constant) and K_3 values (intrinsic equilibrium dissociation constants) specific to the individual modulator. The choice of model (one or two sites per dimer interface) was based on the slope of the curve and the fit of the model to the data. As shown in Figure 3B, the dependence of dimerization on the concentration of allosteric modulator can have quite different slopes depending upon which modulator is used. As shown previously,¹¹ those modulators that bind to one site per dimer interface exhibit a relatively shallow slope (HFMZ in Figure 3B),¹² while those that bind to two sites show a much steeper slope (cyclothiazide **1**).²⁵ This is not due to cooperativity of modulator binding but rather a consequence of the fact that the two-site model assumes that dimerization is stabilized further with each successive occupancy. Two of the compounds in Figure 1 (**5** and **3**) show a steeper slope consistent with binding to two sites per dimer interface (consistent with the crystal

structures of **5**²³ and **3**, see below in this paper). Reference compound **5** (K_3 of 9×10^{-7} M) is somewhat more potent than reference compound **3** (K_3 of 2×10^{-6} M). This is in contrast to the calcium flux experiments that show a considerably larger difference between the two compounds. The SAXS experiments are not directly comparable to measurements of the intact receptor because the mechanism involves the dimerization of two identical soluble proteins with an extremely weak dimerization constant (approximately 32 mM), leading to an EC_{50} considerably higher than that measured in the intact receptor. K_3 is the intrinsic binding constant for the interaction of the modulator with the GluA2-LBD-N775S dimer. This, in principle, should be the same in the intact receptor. The difference is that in the intact receptor, the two monomers within the dimer are held in close proximity by the structure, and the formation of the dimer interface can be seen as a favorable conformation transition rather than a weak protein–protein interaction involving the diffusion of two independent proteins. For this reason, the EC_{50} measured in the intact receptor is generally lower than that observed in the SAXS measurements. (See the supplement to Ptak et al.¹¹ for a further discussion of this point.) The calcium flux measurements suggest that compound **11m** is several orders more potent than the reference compounds **3** and **5**. This raised a difficulty in the SAXS measurements because typical protein concentrations are higher than the affinity for this compound, suggesting that modulator rather than protein would be limiting. This was approached by using several low concentrations of GluA2-LBD-N775S and signal averaging three independent data sets. The shapes of the dimerization curves indicated that at some of the concentrations tested, the modulator was indeed limiting. This is reflected in the shape of the dimerization curves, which become increasingly steep as the protein concentration increases (Figure 3B). By using a numerical fitting routine described in the Experimental Section that takes into account the limiting modulator concentration, the affinity of compound **11m** could be determined for a model assuming one binding site per dimer interface. At the lowest protein concentration, the dimerization slope was similar to that of HFMZ, further supporting a model with one site per dimer interface, consistent with the crystal structure described below. The four curves for compound **11m** shown in Figure 3B were generated with a K_4 of 32 mM and K_3 of 5×10^{-11} M. The change in the shape of the curve with increasing concentration does not reflect an increase in stoichiometry but is solely a predictable consequence of a limiting modulator concentration. In fact, this change in shape provided a significant constraint on the value of K_3 . Overall, the SAXS measurements show that compound **3** and **5** both bind in two copies per dimer interface and are of considerably lower affinity than compound **11m**, which occupies only one site per dimer interface.

Structure Determination. To investigate the binding mode of the highly potent compound **11m**, and especially how the larger substituent in the 7-position is located in the binding site, the GluA2-LBD was crystallized in complex with **11m**. In addition, the GluA2-LBD-L504Y-N775S was crystallized with the reference compound **3**. This compound differs from previously crystallized BTDs as it contains a fluoro-ethyl group at *N*-4 and chlorine at the *C*-7 position. The structures were determined at 2.00 and 1.78 Å, respectively (Table 2).

GluA2-LBD with 11m. The GluA2-LBD in complex with **11m** crystallized with three molecules in the asymmetric unit,

forming two biological dimers (molA/molB (Figure 4A) and molC/symmetry-related molC). Glutamate is present in the orthosteric-binding site of all three protein molecules, leading to D1-D2 domain closures of 19–21°.

Unambiguous electron density was identified at the interface of both dimers corresponding to **11m** (Figure 4B). As suggested by the Hill coefficient in the calcium flux assays and the shape of the dimerization curve in the SAXS data, only one molecule of **11m** can occupy the modulator-binding sites at a time, leading to two alternative binding modes with the BTD-scaffold positioned in one of the two binding sites seen in the structure of GluA2-LBD with compound **5**.²³ Due to the symmetrical dimer, the binding mode of the two molecules of **11m** is rotated 180° relative to each other. The occupancy of the modulator and corresponding water molecules was refined to 0.55/0.45 for molA/molB and 0.46 for molC. The 7-substituent occupies the second binding site together with three water molecules (W1–W3), occupying the same space in the binding site as the sulfonamide of **11m** in the alternate binding mode. Compound **11m** belongs to the shifted thiazide class of modulators, with the BTD scaffold primarily located in subsite C but the 7-(3'-methoxyphenoxy) substituent spanning subsite A with the 3'-methoxy moiety oriented toward subsite B' (Figure 4C). Previous studies of thiazide modulators (class *i* and *ii*) have shown that most of these compounds do not reach into subsite A and thus can bind two molecules in the dimer interface.^{12,26}

One hydrogen bond is formed from the sulfonamide N atom of **11m** to the backbone O atom of Pro515. The three water molecules (W1–W3) found to occupy the second BTD binding site together with the 7-(3'-methoxyphenoxy) substituent do not form polar contacts with the 7-(3'-methoxyphenoxy) substituent, but instead establish a network of polar contacts from the backbone O atom of Pro515 on one side of the dimer to the backbone N atom of Gly752 and O atom Ile502 on the other side (Figure 4C). Multiple nonpolar interactions are possible from **11m** to surrounding residues within 4 Å. The BTD scaffold forms contact to Lys514, Pro515, Phe516, Met517, Ser518, Asn775, and Leu780 from one protein chain and Ile502, Pro515, Ser518, Ser750, Lys751, and Gly752 from the opposite protein chain in the dimer comprising molA and molB. Almost identical interactions are seen in the symmetry-generated dimer (molC/sym-molC); however, in molC, the contact to Ser518 is replaced by a contact to Leu772 in the same chain. Although no polar contacts are established from the 7-(3'-methoxyphenoxy) substituent to surrounding residues, the substituent engages in nonpolar interactions with nine of the 12 same residues as the BTD scaffold: Ser750 and Lys751 from one protein chain, and Pro515, Phe516, Met517, Ser518, Gly752, Asn775, and Leu780 from the opposite chain. Thus, binding of one molecule of **11m** to a large extent recreates the interactions seen when two molecules of **5** bind in the dimer interface. In addition, the benzene ring of the 7-phenoxy substituent is positioned to form pi-stacking interactions with the backbone amide bonds between Lys751–Gly752 in one subunit and Met517–Ser518 in the other subunit. These observations, combined with smaller entropy loss upon binding of one instead of two molecules, may explain the 40-fold better potency of **11m** ($EC_{50} = 2.0$ nM) compared to **5** ($EC_{50} = 813$ nM).

The activity for the newly synthesized series of compounds was found to correlate with the position of the substituent on the 7-phenoxy moiety in the following order: *meta* > *para* >

Table 2. Crystal Data, Data Collection, and Refinement Statistics for the GluA2-LBD-L504Y–N775S in Complex with **3** and GluA2-LBD in Complex with **11m**

	complex	
	3	11m
Crystal Data		
PDB entry	5O9A	5OEW
space group	$P2_1$	$P2_12_12$
unit cell: a, b, c (Å)	47.31, 98.41, 121.79	114.70, 164.37, 47.33
units cell: β (°)	90.53	90
molecules in a.u. ^a	4	3
Data Collection		
wavelength (Å)	0.979	1.000
resolution ^b (Å)	49.20–1.78 (1.88–1.78)	29.27–2.00 (2.11–2.00)
no. of unique reflections	106 755 (15 582)	61 361 (8 859)
average redundancy	3.7 (3.6)	4.1 (4.1)
completeness (%)	100 (100)	99.8 (99.8)
R_{merge}^c	0.063 (0.377)	0.087 (0.313)
$I/\sigma I$	10.4 (2.0)	6.5 (2.0)
Wilson B (Å ²)	13.6	17.5
Refinement		
amino acid residues	263/264/263/260	261/259/261
glutamate/modulator	4/4	3/2
acetate/sulfate/Zn/Cl	–/16/–/7	4/–/18/–
glycerol/PEG/ethylene glycol/citrate/water	3/1/1/1/1186	–/–/–/–/522
$R_{\text{work}}^d/R_{\text{free}}^e$	0.15/0.18	0.17/0.19
average B values (Å ²) for amino acid residues	18/25/17/24	27/28/23
average B values (Å ²) for glutamate/modulator	12/15	18/15
average B values (Å ²) for acetate/sulfate/Zn/Cl	–/60/–/53	46/–/64/–
average B values (Å ²) for glycerol/PEG/ethylene glycol/citrate/water	49/47/46/30/29	–/–/–/–/34
RMSDs: bond lengths (Å)	0.01	0.03
RMSDs: angles (°)	0.79	0.61
Ramachandran plot (%): outliers	0	0
Ramachandran plot (%): favored	99.2	99.4
rotamer outliers ^f	1.0	1.0
C β outliers ^f (%)	0	0
clash score ^f	0.74	0.56

^aa.u.: asymmetric unit of the crystal. ^bValues in parentheses correspond to the outermost resolution shell. ^c R_{merge} is calculated as follows: $I_i(hkl)$ is the intensity of an individual measurement of the reflection with Miller indices hkl , and $I(hkl)$ is the intensity from multiple observations. $R_{\text{merge}} = \frac{\sum_{hkl} \sum_i |I_i(hkl) - I(hkl)|}{\sum_{hkl} \sum_i I_i(hkl)}$. ^d $R_{\text{work}} = \frac{\sum_{hkl} |F_{\text{obs}} - F_{\text{calc}}|}{\sum_{hkl} |F_{\text{obs}}|}$ where F_{obs} and F_{calc} are the observed and calculated structure factor amplitudes, respectively, for reflection hkl . ^e R_{free} is equivalent to R_{work} but is calculated with 5% of reflections omitted from the refinement process. ^fMolProbity statistics.⁴⁵

ortho. From the structure of **11m** bound to GluA2-LBD, this ranking might be explained. Introduction of substituents in the *ortho* position, even a methyl group, would require changes in the conformation or binding mode of the modulator or protein rearrangements to avoid steric clash with Met517–Ser518. Likewise, large substituents in the *para* position will lead to clash with protein residues and interference with the intermolecular hydrogen bond between the side-chain ND2 atom of Asn775 and the backbone O atom of Ser750, whereas the *meta* position of the 7-phenoxy moiety holds the most space for introduction of substituents. The *m*-OCH₃ in **11m** has several van der Waals contacts to both protein molecules, which would be less with an *m*-CH₃ group (**11j**). This might explain the better potency of **11m** compared to **11j**. However, an *m*-CN as in **11o** would lead to steric clash with the protein and would require changes in the conformation or binding mode of the modulator or protein rearrangements.

GluA2-LBD-L504Y–N775S with 3. Compound **3** was crystallized in complex with GluA2-LBD-L504Y–N775S in the presence of glutamate. This mutant has previously been used in

several studies addressing modulator binding (see Krintel et al.¹⁶): the complex crystallized with four molecules in the asymmetric unit, forming two biological dimers (molA/molB (Figure 5A) and molC/molD). Glutamate binds in all four protein molecules, leading to D1–D2 domain closures of 20–22°.

Unambiguous electron density was identified at the interface of both dimers corresponding to **3** (Figure 5B). Two molecules of **3** bind at the dimer interface in subsite C, as seen with other BTD containing compounds like **5**²³ and **12**.²¹ One hydrogen bond is formed from the sulfonamide N atom of **3** to the backbone O atom of Pro515 (Figure 5B) as also seen in the GluA2-LBD structure with **11m**. Ser518 adopts two different side-chain conformations in all four protein molecules, one pointing away from the modulator and one pointing toward it. When the side chain of Ser518 points toward the modulator, it allows for the formation of a hydrogen bond at the 7-chlorine atom (distances of 3.1–3.2 Å). However, the occupancy of the side chain in this conformation is only 30%, consistent with the fact that the chlorine atom is expected to be a poor proton

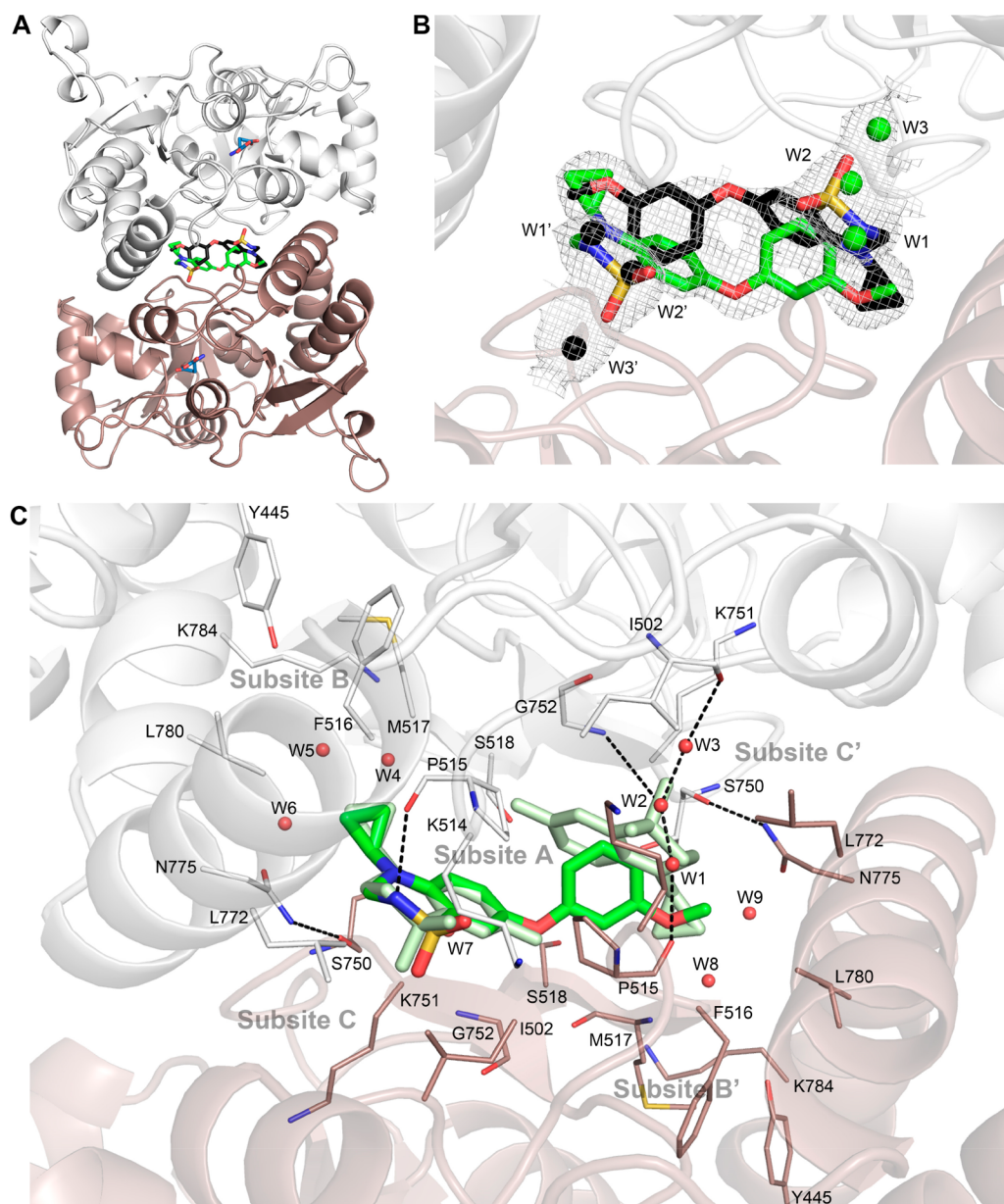


Figure 4. Structure of GluA2-LBD in complex with glutamate and the AMPAR potentiator **11m**. (A) Cartoon representation of the GluA2-LBD dimer (molA in white and molB in dark salmon) with glutamate shown in blue sticks representation and the two binding orientations of **11m** in green and black, respectively. Nitrogen atoms are blue, oxygen atoms red, and sulfur atoms yellow. (B) Compound **11m** binds to one site in the dimer interface. However, because of the symmetry of the dimer interface, two overlapping copies of the compound are observed in the crystal structure, only one of which is present in any given dimer. A $2F_o - F_c$ OMIT map (gray mesh, contoured at 0.5σ and carved around the modulator at 2.0 \AA) is shown with the two orientations of **11m**. Six water molecules are shown as spheres: green water molecules are present together with **11m** in green orientation and black water molecules with **11m** in black orientation. (C) Compound **11m** primarily occupies subsites A and C in the allosteric binding site. GluA2 residues are shown in line representation, green orientation of **11m** in sticks representation. Hydrogen bonds are shown as dashed black lines and water molecules within 4 \AA of **11m** as red spheres. The binding mode of two molecules of **5** (light green sticks) is shown for comparison.

acceptor.²⁷ Introduction of larger substituents at the 7-position is likely to cause steric clash with Met517 and Ser518, in agreement with previous observations that the potency decreases with iodine and methyl substituents.¹⁹ However, the introduction of a smaller substituent in the 7-position, such as the fluorine analogue of **3** ($EC_{2x} = 11.3 \mu\text{M}$), leads to an increase in potency compared to **3** with chlorine in the 7-position ($EC_{2x} = 18.8 \mu\text{M}$).²⁸

The alkyl chain of **3** is bent to a U-shaped conformation, where the fluorine atom points toward the chlorine atom of the

neighboring modulator molecule with a $\text{C}-\text{Cl}\cdots\text{F}$ bond angle of 165° (Figure 5B). The $\text{Cl}-\text{F}$ distances between the two neighboring molecules of **3** are $4.1\text{--}4.4 \text{ \AA}$. Chlorine, due to the charge distribution of a soft halogen, has an electropositive tip, called sigma-hole (Figure 5C).^{29,30} This leads to a favorable interaction between the chlorine and the electronegative fluorine. The aromatic ring system in **3** shows van der Waals contacts to the 7-chlorine atom of the neighboring molecule of **3** with a shortest distance of 3.4 \AA .

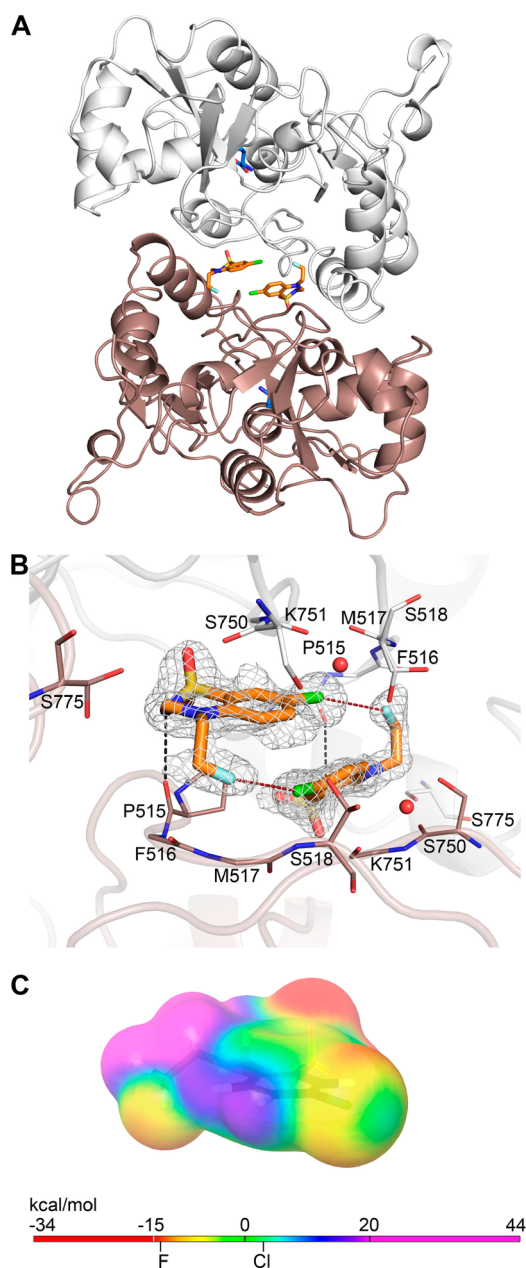


Figure 5. Structure of GluA2-LBD-L504Y-N775S in complex with glutamate and the AMPAR potentiator **3**. (A) Cartoon representation of the GluA2-LBD-L504Y-N775S dimer (molA in white and molB in dark salmon) with glutamate shown in a blue stick representation and two molecules of **3** in orange. Nitrogen atoms are blue, oxygen atoms red, and sulfur atoms yellow. (B) The two molecules of compound **3** primarily occupies subsites C in the allosteric binding site. GluA2 residues are shown in line representation, **3** in stick representation, and water molecules within 3.5 Å of modulator as red spheres. Hydrogen bonds up to 3.2 Å are shown as dashed black lines. F-Cl distances (4.1–4.4 Å) are indicated as red dashed lines. A $2F_o - F_c$ OMIT map is shown as a gray mesh, contoured at 1σ and carved around the modulator at 1.8 Å. (C) The electrostatic potential map on the electron density map of **3** is represented in rainbow colors. Potentials below -15 kcal/mol are shown with red and above $+20$ in magenta. The electropositive tip (3 kcal/mol) of chlorine can make a halogen bond to the electronegative (-14 kcal/mol) fluorine. The electrostatic potential of **3** was calculated using Jaguar in MAESTRO (v.10.1; Schrödinger, LLC, New York, NY, 2015) with the cc-PVDZ basis set and B3LYP hybrid potential.

NMR Spectroscopy. The GluA2-LBD-N775S was uniformly labeled with ^{15}N and, on an 800 MHz spectrometer, $^1\text{H},^{15}\text{N}$ -HSQC-TROSY spectra were collected in the presence and absence of $90\ \mu\text{M}$ compound **11m**. A significant fraction of the protein was dimerized as indicated by line broadening and the presence of new broadened peaks. Peaks in the dimer interface formed by the binding of **11m** were significantly shifted and not readily assigned in this spectrum. However, on the periphery of the dimer interface, the change in chemical environment was less pronounced such that the peak shifts were smaller. An example is Gly760 (Figure 6), which clearly

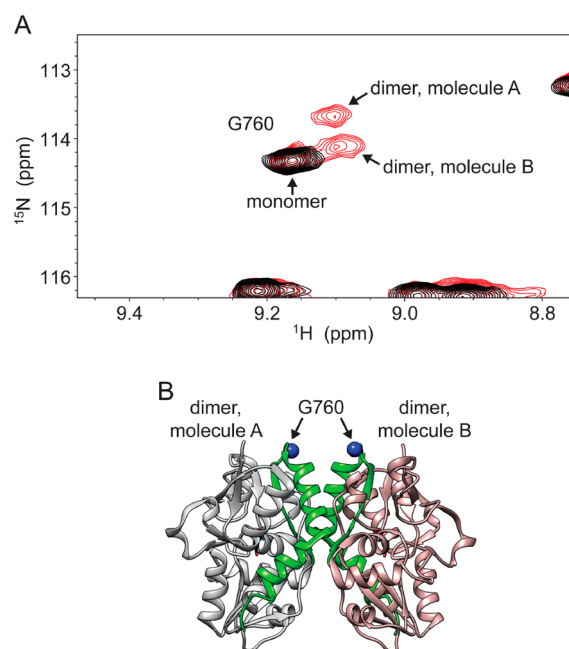


Figure 6. GluA2-LBD-N775S dimerization using NMR spectroscopy. (A) Portion of the $^1\text{H},^{15}\text{N}$ -HSQC-TROSY spectra at 800 MHz showing monomeric GluA2-LBD-N775S in black and the partially dimerized spectrum bound to compound **11m** in red. (B) Structure of the dimer of GluA2-LBD-N775S (PDB entry 3DP6) with G760 shown as a blue sphere.

shows two new peaks formed by the binding of compound **11m** and dimerization. Simple dimerization would not produce two new peaks because the dimer interface is symmetrical. Consistent with the crystal structure and SAXS results, the binding of one molecule of compound **11m** to the dimer interface breaks that symmetry, producing two peaks.

CONCLUSION

With the aim of exploring the influence of monosubstitution of the phenoxy ring introduced at the 7-position of the benzothiadiazine dioxide scaffold, we developed a synthetic pathway giving access to the preparation of 15 compounds. We also developed a new medium-throughput fluorimetric assay in order to screen this series.

The first part of the work led to highlight the high potency of **11m**, with an $\text{EC}_{50} = 2.0$ nM (calcium flux experiment); this *in vitro* activity was found to be the highest in comparison with our previous lead structures. Interestingly, the activity curves obtained for the new compounds shared a much lower Hill coefficient than the curves obtained with reference compounds from our library. Considering this interesting activity profile,

attention was thus focused on the characterization of the binding mode of the most active compound **11m** in the series via complementary SAXS, NMR, and crystallography.

SAXS data first corroborated the high affinity of **11m** and confirmed that this compound occupies only one site per dimer interface, contrary to most benzothiadiazine dioxides developed as AMPAR potentiators. Structure determination of GluA2-LBD in complex with glutamate and **11m** confirmed that only one molecule of **11m** binds at the dimer interface and revealed the detailed binding mode. Compound **11m** primarily occupies subsites A and C. Results obtained with NMR spectroscopy were found to be consistent with the X-ray and SAXS data.

From these observations, compound **11m** behaves as two molecules of the reference compound **5**, since **11m** is able to recreate the interaction observed after two molecules of compound **5** binds into the allosteric pocket. Altogether, the data collected in this second part confirmed that compound **11m** belongs to a singular subclass of the benzothiadiazine dioxides developed so far.

The binding mode of compound **3** was characterized using SAXS and crystallography. Compound **3** binds in two copies per dimer interface and occupies subsites C within the allosteric pocket. A chlorine–fluorine interaction between the two neighboring molecules was found.

This study suggests that 3,4-dihydro-2*H*-1,2,4-benzothiadiazine 1,1-dioxide is (still) a very interesting scaffold to develop new powerful AMPAR potentiators. Keeping this idea in mind, efforts should now be focused toward the design of new BTDS in order to further map the GluA2-LBD and develop powerful pharmacological tools useful to refine knowledge of the AMPAR biology.

EXPERIMENTAL SECTION

General Procedures. Melting points were determined on a Büchi Tottoli capillary apparatus and were uncorrected. The ^1H and ^{13}C NMR spectra were recorded on a Bruker Avance (^1H : 500 MHz, ^{13}C : 125 MHz) instrument using deuterated dimethyl sulfoxide ($\text{DMSO-}d_6$) as the solvent with tetramethylsilane (TMS) as an internal standard; chemical shifts were reported in δ values (ppm) relative to that of internal TMS. The abbreviations s = singlet, d = doublet, t = triplet, q = quadruplet, m = multiplet, and bs = broad singlet were used throughout. Elemental analyses (C, H, N, S) were realized on a Thermo Scientific Flash EA 1112 elemental analyzer and were within $\pm 0.4\%$ of the theoretical values for carbon, hydrogen, and nitrogen; a higher tolerance ($\pm 0.75\%$) was admitted for sulfur, considering its corresponding peak shape. This analytical method certified a purity of $\geq 95\%$ for each tested compound. All reactions were routinely checked by TLC on silica gel (Merck 60 F254).

7-Methoxy-4-methyl-4*H*-1,2,4-benzothiadiazine 1,1-Dioxide (8). The mixture of 7-methoxy-4*H*-1,2,4-benzothiadiazine 1,1-dioxide (**7**)¹⁹ (10.0 g, 47.2 mmol), potassium carbonate (20 g), and methyl iodide (15 mL) in acetonitrile (300 mL) was heated at 60 °C for 3 h. The solvent was removed by distillation under reduced pressure, and the residue was suspended in water (400 mL). The resulting insoluble material was collected by filtration, washed with water, dried, and recrystallized in ethyl acetate (8.6 g, 81% yield): mp 204–206 °C (lit.¹⁸ 205–209 °C); ^1H NMR ($\text{DMSO-}d_6$, 500 MHz) δ 3.61 (s, 3H, NCH_3), 3.87 (s, 3H, 7-OCH₃), 7.31 (d, $J = 2.9$ Hz, 1H, 8-*H*), 7.38 (dd, $J = 9.3, 2.9$ Hz, 1H, 6-*H*), 7.49 (d, $J = 9.3$ Hz, 1H, 5-*H*), 8.01 (s, 1H, 3-*H*); ^{13}C NMR ($\text{DMSO-}d_6$) δ 38.0 (NCH_3), 56.0 (O–CH₃), 106.1 (C-8), 118.6 (C-5), 120.9 (C-6), 123.6 (C-4a), 129.6 (C-8a), 150.3 (C-3), 157.4 (C-7).

7-Methoxy-4-methyl-3,4-dihydro-2*H*-1,2,4-benzothiadiazine 1,1-Dioxide (9). The solution of 4-methyl-7-methoxy-2*H*-1,2,4-benzothiadiazine 1,1-dioxide (**8**) (6.0 g, 27 mmol) in 2-propanol (300 mL) was supplemented under stirring with sodium borohydride

(3.0 g, 80 mmol). After 45 min of stirring the mixture at room temperature, the solvent was removed by distillation under reduced pressure and the residue was suspended in water (250 mL). The alkaline suspension was adjusted to pH 7 with 0.1 N HCl and extracted 3-fold with chloroform (3 \times 250 mL). The combined organic layers were dried over MgSO_4 and filtered. The filtrate was concentrated to dryness under reduced pressure, and the residue of the title compound was recrystallized in methanol/water 1:2 (4.7 g, 78% yield): mp 127–129 °C (lit.¹⁸ 126–128 °C); ^1H NMR ($\text{DMSO-}d_6$, 500 MHz) δ 2.89 (s, 3H, NCH_3), 3.73 (s, 3H, 7-OCH₃), 4.57 (s, 2H, 3-CH₂), 6.87 (d, $J = 9.2$ Hz, 1H, 5-*H*), 7.04 (d, $J = 3.0$ Hz, 1H, 8-*H*), 7.09 (dd, $J = 9.2, 3.0$ Hz, 1H, 6-*H*), 8.05 (s, 1H, 3-*H*); ^{13}C NMR ($\text{DMSO-}d_6$) δ 36.7 (NCH_3), 55.6 (O–CH₃), 62.4 (C-3), 107.4 (C-8), 116.2 (C-5), 121.0 (C-6), 123.3 (C-4a), 138.8 (C-8a), 150.5 (C-7).

7-Hydroxy-4-methyl-3,4-dihydro-2*H*-1,2,4-benzothiadiazine 1,1-Dioxide (10a). The solution of 7-methoxy-4-methyl-3,4-dihydro-2*H*-1,2,4-benzothiadiazine 1,1-dioxide (**9**) (5.0 g, 21.9 mmol) in dichloromethane (200 mL) was cooled at –30 °C and then supplemented with boron tribromide (16 mL). After 6 h of stirring the mixture at room temperature, water (200 mL) was carefully poured in the reaction mixture and the organic solvent was removed by distillation under reduced pressure. The aqueous layer was extracted with ethyl acetate (3 \times 200 mL). The collected organic layers were dried over MgSO_4 and filtered. The filtrate was evaporated to dryness, and the residue was crystallized in dichloromethane and dried (76% yield): mp 165–166 °C (lit.¹⁸ 168–172 °C); ^1H NMR ($\text{DMSO-}d_6$) δ 2.85 (s, 3H, NCH_3), 4.52 (s, 2H, 3-CH₂), 6.78 (d, $J = 9.8$ Hz, 1H, 5-*H*), 6.91 (m, 2H, 6-*H*/7-*H*), 7.99 (bs, 1H, 2-*H*), 9.31 (bs, 1H, 7-OH); ^{13}C NMR ($\text{DMSO-}d_6$) δ 36.9 (NCH_3), 62.5 (C-3), 109.2 (C-8), 116.5 (C-5), 121.4 (C-6), 123.8 (C-4a), 137.6 (C-8a), 148.6 (C-7).

General Synthetic Pathway to Obtain 7-Phenoxy-Substituted 4-Alkyl-3,4-dihydro-2*H*-1,2,4-benzothiadiazine 1,1-Dioxides 11. A solution of the appropriate 4-alkyl-3,4-dihydro-2*H*-1,2,4-benzothiadiazine 1,1-dioxide **10** (1.7 mmol) in dichloromethane (60 mL) and pyridine (10 drops), molecular sieves (5 g), the adequately substituted phenyl boronic acid (2.5 mmol), and copper(II) acetate (2.5 mmol) was stirred at 40 °C. After 5 h, dichloromethane was added to the medium and the solid was removed by filtration. The filtrate was evaporated under reduced pressure before the addition of acidic water (50 mL). The resulting suspension was extracted with ethyl acetate (3 \times 50 mL). The organic phases were collected and dried over anhydrous MgSO_4 . The removal of the solvent followed by flash column chromatography on silica gel (dichloromethane) and subsequent recrystallization (dichloromethane/petroleum ether 5:15) afforded the pure **11** compounds (yields 13–74%).

4-Methyl-7-phenoxy-3,4-dihydro-2*H*-1,2,4-benzothiadiazine 1,1-Dioxide (11a): 74% yield, mp 143.5–145.5 °C; ^1H NMR ($\text{DMSO-}d_6$) δ 2.94 (s, 3H, NCH_3), 4.65 (s, 2H, 3-CH₂), 6.94 (m, 3H, 5-*H*/2'-*H*/6'-*H*), 7.12 (m, 2H, 4'-*H*/8-*H*), 7.22 (dd, $J = 9.1, 2.8$ Hz, 1H, 6-*H*), 7.38 (t, $J = 7.9$ Hz, 1H, 3'-*H*/5'-*H*), 8.11 (bs, 1H, NH); ^{13}C NMR ($\text{DMSO-}d_6$) δ 36.4 (NCH_3), 62.3 (C-3), 114.3 (C-8), 116.0 (C-5), 117.5 (C-2'/C-6'), 123.0 (C-8a), 123.1 (C-4'), 125.2 (C-6), 130.0 (C-3'/C-5'), 140.9 (C-4a), 146.2 (C-7), 157.5 (C-1'). Anal. (C₁₄H₁₄N₂O₃S) Calcd: C, 57.91; H, 4.86; N, 9.65; S, 11.04. Found: C, 57.96; H, 4.93; N, 10.04; S, 10.80.

4-Methyl-7-(2-methylphenoxy)-3,4-dihydro-2*H*-1,2,4-benzothiadiazine 1,1-Dioxide (11b): 25% yield, mp 166–168 °C; ^1H NMR ($\text{DMSO-}d_6$) δ 2.20 (s, 3H, CH₃), 2.93 (s, 3H, NCH_3), 4.63 (s, 2H, 3-CH₂), 6.79 (d, $J = 8.1$ Hz, 1H, 6'-*H*), 6.93 (d, $J = 9.2$ Hz, 1H, 5-*H*), 6.96 (d, $J = 2.9$ Hz, 1H, 8-*H*), 7.08 (td, $J = 7.4, 1.0$ Hz, 1H, 4'-*H*), 7.15 (dd, $J = 9.2, 3.0$ Hz, 1H, 6-*H*), 7.20 (td, $J = 7.6, 1.2$ Hz, 1H, 5'-*H*), 7.32 (d, $J = 7.5$ Hz, 1H, 3'-*H*), 8.11 (s, 1H, NH); ^{13}C NMR ($\text{DMSO-}d_6$) δ 15.8 (CH₃), 36.5 (NCH_3), 62.3 (C-3), 112.3 (C-8), 116.2 (C-5), 118.2 (C-6'), 123.1 (C-8a), 123.8 (C-4'), 124.1 (C-6), 127.4 (C-5'), 128.5 (C-2'), 131.5 (C-3'), 140.3 (C-4a), 147.3 (C-7), 154.6 (C-1'). Anal. (C₁₅H₁₆N₂O₃S) Calcd: C, 59.19; H, 5.30; N, 9.20; S, 10.53. Found: C, 58.90; H, 5.24; N, 8.87; S, 10.21.

4-Methyl-7-(3-methylphenoxy)-3,4-dihydro-2*H*-1,2,4-benzothiadiazine 1,1-Dioxide (11c): 35% yield, mp 173.5–175.5 °C; ^1H NMR

(DMSO- d_6) δ 2.28 (s, 3H, CH₃), 2.94 (s, 3H, NCH₃), 4.65 (d, J = 8.1 Hz, 2H, 3-CH₂), 6.73 (dd, J = 8.1, 2.0 Hz, 1H, 4'-H), 6.76 (s, 1H, 2'-H), 6.93 (d, J = 9.1 Hz, 2H, 5-H/6'-H), 7.11 (d, J = 2.9 Hz, 1H, 8-H), 7.20 (dd, J = 9.1, 2.9 Hz, 1H, 6-H), 7.25 (t, J = 7.8 Hz, 1H, 5'-H), 8.13 (t, J = 8.1 Hz, 1H, NH); ¹³C NMR (DMSO- d_6) δ 20.9 (CH₃), 36.4 (NCH₃), 62.3 (C-3), 114.3 (C-8), 114.6 (C-4'), 116.0 (C-5), 118.0 (C-2'), 123.0 (C-8a), 123.8 (C-6'), 125.5 (C-6), 129.7 (C-5'), 139.7 (C-4a), 140.8 (C-3'), 146.3 (C-7), 157.5 (C-1'). Anal. (C₁₅H₁₆N₂O₃S) Calcd: C, 59.19; H, 5.30; N, 9.20; S, 10.53. Found: C, 59.18; H, 5.37; N, 9.18; S, 9.88.

4-Methyl-7-(4-methylphenoxy)-3,4-dihydro-2H-1,2,4-benzothiadiazine 1,1-Dioxide (11d): 25% yield, mp 137–139 °C; ¹H NMR (DMSO- d_6) δ 2.28 (s, 3H, CH₃), 2.93 (s, 3H, NCH₃), 4.63 (s, 2H, 3-CH₂), 6.86 (d, J = 8.5 Hz, 2H, 2'-H/6'-H), 6.92 (d, J = 9.2 Hz, 1H, 5-H), 7.06 (d, J = 2.9 Hz, 1H, 8-H), 7.19 (m, 3H, 6-H/3'-H/5'-H), 8.11 (s, 1H, NH); ¹³C NMR (DMSO- d_6) δ 20.2 (CH₃), 36.5 (NCH₃), 62.3 (C-3), 113.5 (C-8), 116.1 (C-5), 117.9 (C-2'/C-6'), 123.0 (C-8a), 125.0 (C-6), 130.4 (C-3'/C-5'), 132.3 (C-4'), 140.6 (C-4a), 147.0 (C-7), 155.0 (C-1'). Anal. (C₁₅H₁₆N₂O₃S) Calcd: C, 59.19; H, 5.30; N, 9.20; S, 10.53. Found: C, 59.02; H, 5.37; N, 9.11; S, 9.92.

4-Methyl-7-(2-methoxyphenoxy)-3,4-dihydro-2H-1,2,4-benzothiadiazine 1,1-Dioxide (11e): 19% yield, mp 150–151.5 °C; ¹H NMR (DMSO- d_6) δ 2.96 (s, 3H, NCH₃), 3.75 (s, 3H, OCH₃), 4.60 (s, 2H, 3-CH₂), 6.87 (d, J = 2.9 Hz, 1H, 8-H), 6.89 (d, J = 9.8 Hz, 1H, 5-H), 6.98 (m, 2H, 5'-H/6'-H), 7.09 (dd, J = 9.2, 2.9 Hz, 1H, 6-H), 7.19 (m, 2H, 3'-H/4'-H), 8.08 (bs, 1H, NH); ¹³C NMR (DMSO- d_6) δ 36.5 (NCH₃), 55.6 (OCH₃), 62.3 (C-3), 110.8 (C-8), 113.5 (C-3'), 116.0 (C-5), 121.0–121.1 (C-5'/C-6'), 122.8 (C-6), 122.9 (C-8a), 125.5 (C-4'), 139.9 (C-4a), 144.0 (C-1'), 148.3 (C-7), 151.1 (C-2'). Anal. (C₁₅H₁₆N₂O₄S) Calcd: C, 56.24; H, 5.03; N, 8.74; S, 10.01. Found: C, 56.12; H, 5.06; N, 8.78; S, 9.95.

4-Methyl-7-(3-methoxyphenoxy)-3,4-dihydro-2H-1,2,4-benzothiadiazine 1,1-Dioxide (11f): 43% yield, mp 143.5–145.5 °C; ¹H NMR (DMSO- d_6) δ 2.95 (s, 3H, NCH₃), 3.73 (s, 3H, OCH₃), 4.65 (s, 2H, 3-CH₂), 6.46 (dd, J = 8.1, 2.0 Hz, 1H, 6'-H), 6.53 (t, J = 2.2 Hz, 1H, 2'-H), 6.69 (dd, J = 8.2, 2.1 Hz, 1H, 4'-H), 6.93 (d, J = 9.2 Hz, 1H, 5-H), 7.15 (d, J = 8.2 Hz, 1H, 8-H), 7.22 (dd, J = 9.1, 2.9 Hz, 1H, 6-H), 7.26 (t, J = 8.2 Hz, 1H, 5'-H), 8.11 (bs, 1H, NH); ¹³C NMR (DMSO- d_6) δ 36.4 (NCH₃), 55.2 (OCH₃), 62.3 (C-3), 103.7 (C-2'), 108.6 (C-4'), 109.4 (C-6'), 114.4 (C-8), 116.0 (C-5), 123.0 (C-8a), 125.6 (C-6), 130.5 (C-5'), 140.9 (C-4a), 146.0 (C-7), 158.7 (C-1'), 160.7 (C-3'). Anal. (C₁₅H₁₆N₂O₄S) Calcd: C, 56.24; H, 5.03; N, 8.74; S, 10.01. Found: C, 56.10; H, 4.99; N, 8.51; S, 9.65.

4-Methyl-7-(4-methoxyphenoxy)-3,4-dihydro-2H-1,2,4-benzothiadiazine 1,1-Dioxide (11g): 27% yield, mp 104–106 °C; ¹H NMR (DMSO- d_6) δ 2.92 (s, 3H, NCH₃), 3.74 (s, 3H, OCH₃), 4.62 (s, 2H, 3-CH₂), 6.91 (d, J = 9.2 Hz, 1H, 5-H), 6.95 (s, 4H, 2'-H/3'-H/5'-H/6'-H), 7.00 (d, J = 2.9 Hz, 1H, 8-H), 7.16 (dd, J = 9.2, 2.9 Hz, 1H, 6-H), 8.10 (bs, 1H, NH); ¹³C NMR (DMSO- d_6) δ 36.5 (NCH₃), 55.4 (OCH₃), 62.3 (C-3), 112.6 (C-8), 115.1 (C-3'/C-5'), 116.1 (C-5), 119.8 (C-2'/C-6'), 123.0 (C-8a), 124.3 (C-6), 140.3 (C-4a), 148.1 (C-7), 150.2 (C-1'), 155.4 (C-4'). Anal. (C₁₅H₁₆N₂O₄S) Calcd: C, 56.24; H, 5.03; N, 8.74; S, 10.01. Found: C, 56.29; H, 4.97; N, 8.50; S, 9.44.

4-Cyclopropyl-7-phenoxy-3,4-dihydro-2H-1,2,4-benzothiadiazine 1,1-Dioxide (11h): 57% yield, mp 198–200 °C; ¹H NMR (DMSO- d_6) δ 0.66 (m, 2H, CH(CH₂)₂), 0.90 (m, 2H, CH(CH₂)₂), 2.51 (m, 1H, CH(CH₂)₂), 4.66 (s, 2H, 3-CH₂), 6.96 (d, J = 7.8 Hz, 2H, 2'-H/6'-H), 7.13 (m, 2H, 4'-H/8-H), 7.25 (dd, J = 9.2, 2.9 Hz, 1H, 6-H), 7.34 (d, J = 9.2 Hz, 1H, 5-H), 7.38 (m, 2H, 3'-H/5'-H), 7.95 (bs, 1H, NH); ¹³C NMR (DMSO- d_6) δ 8.4 (CH(CH₂)₂), 29.8 (CH(CH₂)₂), 61.1 (C-3), 114.2 (C-8), 116.7 (C-5), 117.7 (C-2'/C-6'), 123.2 (C-4'), 123.4 (C-8a), 125.1 (C-6), 130.0 (C-3'/C-5'), 140.8 (C-4a), 147.1 (C-7), 157.4 (C-1'). Anal. (C₁₆H₁₆N₂O₃S) Calcd: C, 60.74; H, 5.10; N, 8.85; S, 10.13. Found: C, 60.49; H, 5.24; N, 9.07; S, 9.58.

4-Cyclopropyl-7-(2-methylphenoxy)-3,4-dihydro-2H-1,2,4-benzothiadiazine 1,1-Dioxide (11i): 44% yield, mp 244–247 °C; ¹H NMR (DMSO- d_6) δ 0.65 (m, 2H, CH(CH₂)₂), 0.89 (m, 2H, CH(CH₂)₂), 2.20 (s, 3H, CH₃), 2.47 (m, 1H, CH(CH₂)₂), 4.64 (d, J = 8.0 Hz, 2H, 3-CH₂), 6.81 (d, J = 8.0 Hz, 1H, 3'-H), 6.95 (d, J = 2.9 Hz, 1H, 8-H), 7.09 (t, J = 7.4 Hz, 1H, 5'-H), 7.19 (dd, J = 9.2, 2.9 Hz, 1H, 6-H), 7.22

(t, J = 7.5 Hz, 1H, 4'-H), 7.32 (d, J = 7.3 Hz, 1H, 6'-H), 7.33 (d, J = 9.2 Hz, 1H, 5-H), 7.94 (t, J = 8.0 Hz, 1H, NH); ¹³C NMR (DMSO- d_6) δ 8.4 (CH(CH₂)₂), 15.8 (CH₃), 29.8 (CH(CH₂)₂), 61.1 (C-3), 112.1 (C-8), 116.7 (C-5), 118.4 (C-3'), 123.4 (C-8a), 123.7 (C-6), 123.9 (C-5'), 127.5 (C-4'), 128.6 (C-2'), 131.6 (C-6'), 140.2 (C-4a), 148.1 (C-7), 154.4 (C-1'). Anal. (C₁₇H₁₈N₂O₃S) Calcd: C, 61.80; H, 5.49; N, 8.48; S, 9.70. Found: C, 62.09; H, 5.62; N, 8.43; S, 9.50.

4-Cyclopropyl-7-(3-methylphenoxy)-3,4-dihydro-2H-1,2,4-benzothiadiazine 1,1-Dioxide (11j): 52% yield, mp 196–197.5 °C; ¹H NMR (DMSO- d_6) δ 0.66 (m, 2H, CH(CH₂)₂), 0.90 (m, 2H, CH(CH₂)₂), 2.28 (s, 3H, CH₃), 2.49 (m, 1H, CH(CH₂)₂), 4.66 (d, J = 3.7 Hz, 2H, 3-CH₂), 6.74 (dd, J = 8.1, 2.3 Hz, 1H, 4'-H), 6.78 (s, 1H, 2'-H), 6.94 (d, J = 7.5 Hz, 1H, 6'-H), 7.11 (d, J = 2.9 Hz, 1H, 8-H), 7.24 (m, 2H, 6-H/5'-H), 7.34 (d, J = 9.2 Hz, 1H, 5-H), 7.96 (bs, 1H, NH); ¹³C NMR (DMSO- d_6) δ 8.4 (CH(CH₂)₂), 20.9 (CH₃), 29.8 (CH(CH₂)₂), 61.0 (C-3), 114.2 (C-8), 114.7 (C-4'), 116.6 (C-5), 118.2 (C-2'), 123.4 (C-8a), 123.9 (C-6'), 125.1 (C-6), 129.7 (C-5'), 139.7 (C-4a), 140.7 (C-3'), 147.1 (C-7), 157.4 (C-1'). Anal. (C₁₇H₁₈N₂O₃S) Calcd: C, 61.80; H, 5.49; N, 8.48; S, 9.70. Found: C, 62.13; H, 5.56; N, 8.53; S, 9.70.

4-Cyclopropyl-7-(4-methylphenoxy)-3,4-dihydro-2H-1,2,4-benzothiadiazine 1,1-Dioxide (11k): 35% yield, mp 188–190 °C; ¹H NMR (DMSO- d_6) δ 0.65 (m, 2H, CH(CH₂)₂), 0.89 (m, 2H, CH(CH₂)₂), 2.28 (s, 3H, CH₃), 2.49 (m, 1H, CH(CH₂)₂), 4.64 (s, 2H, 3-CH₂), 6.87 (d, J = 8.5 Hz, 2H, 2'-H/6'-H), 7.05 (d, J = 2.9 Hz, 1H, 8-H), 7.19 (d, J = 8.3 Hz, 2H, 3'-H/5'-H), 7.22 (dd, J = 9.2, 2.9 Hz, 1H, 6-H), 7.33 (d, J = 9.2 Hz, 1H, 5-H), 7.95 (s, 1H, NH); ¹³C NMR (DMSO- d_6) δ 8.4 (CH(CH₂)₂), 20.2 (CH₃), 29.8 (CH(CH₂)₂), 61.1 (C-3), 113.4 (C-8), 116.6 (C-5), 118.0 (C-2'/C-6'), 123.4 (C-8a), 124.6 (C-6), 130.4 (C-3'/C-5'), 132.4 (C-4'), 140.5 (C-4a), 147.8 (C-7), 154.9 (C-1'). Anal. (C₁₇H₁₈N₂O₃S) Calcd: C, 61.80; H, 5.49; N, 8.48; S, 9.70. Found: C, 61.86; H, 5.63; N, 8.79; S, 9.29.

4-Cyclopropyl-7-(2-methoxyphenoxy)-3,4-dihydro-2H-1,2,4-benzothiadiazine 1,1-Dioxide (11l): 17% yield, mp 209–212 °C; ¹H NMR (DMSO- d_6) δ 0.63 (m, 2H, CH(CH₂)₂), 0.88 (m, 2H, CH(CH₂)₂), 2.46 (m, 1H, CH(CH₂)₂), 3.75 (s, 3H, OCH₃), 4.61 (s, 2H, 3-CH₂), 6.86 (d, J = 2.9 Hz, 1H, 8-H), 6.99 (m, 2H, 5'-H/6'-H), 7.13 (dd, J = 9.2, 3.0 Hz, 2H, 6-H), 7.19 (m, 2H, 3'-H/4'-H), 7.29 (d, J = 9.2 Hz, 1H, 5-H), 7.92 (s, 1H, NH); ¹³C NMR (DMSO- d_6) δ 8.3 (CH(CH₂)₂), 29.8 (CH(CH₂)₂), 55.6 (OCH₃), 61.1 (C-3), 110.6 (C-8), 113.5 (C-3'), 116.5 (C-5), 121.1 (C-5'/C-6'), 122.5 (C-6), 123.2 (C-8a), 125.6 (C-4'), 139.8 (C-4a), 143.8 (C-1'), 149.1 (C-7), 151.1 (C-2'). Anal. (C₁₇H₁₈N₂O₄S) Calcd: C, 58.94; H, 5.24; N, 8.09; S, 9.25. Found: C, 59.03; H, 5.43; N, 8.46; S, 8.67.

4-Cyclopropyl-7-(3-methoxyphenoxy)-3,4-dihydro-2H-1,2,4-benzothiadiazine 1,1-Dioxide (11m): 31% yield, mp 150–152 °C; ¹H NMR (DMSO- d_6) δ 0.66 (m, 2H, CH(CH₂)₂), 0.90 (m, 2H, CH(CH₂)₂), 2.51 (m, 1H, CH(CH₂)₂), 3.74 (s, 3H, OCH₃), 4.66 (s, 2H, 3-CH₂), 6.47 (dd, J = 8.2, 1.7 Hz, 1H, 6'-H), 6.54 (t, J = 2 Hz, 1H, 2'-H), 6.70 (dd, J = 8.2, 1.9 Hz, 1H, 4'-H), 7.14 (d, J = 2.7 Hz, 1H, 8-H), 7.25 (d, J = 9 Hz, 1H, 6-H), 7.27 (t, J = 8.3 Hz, 1H, 5'-H), 7.34 (d, J = 9.2 Hz, 1H, 5-H), 7.97 (bs, 1H, NH); ¹³C NMR (DMSO- d_6) δ 8.4 (CH(CH₂)₂), 29.8 (CH(CH₂)₂), 55.3 (OCH₃), 61.1 (C-3), 103.9 (C-2'), 108.7 (C-4'), 109.5 (C-6'), 114.4 (C-8), 116.6 (C-5), 123.4 (C-8a), 125.2 (C-6), 130.5 (C-5'), 140.9 (C-4a), 146.8 (C-7), 158.6 (C-1'), 160.7 (C-3'). Anal. (C₁₇H₁₈N₂O₄S) Calcd: C, 58.94; H, 5.24; N, 8.09; S, 9.25. Found: C, 58.60; H, 5.24; N, 8.44; S, 9.20.

4-Cyclopropyl-7-(4-methoxyphenoxy)-3,4-dihydro-2H-1,2,4-benzothiadiazine 1,1-Dioxide (11n): 47% yield, mp 161–162.5 °C; ¹H NMR (DMSO- d_6) δ 0.64 (m, 2H, CH(CH₂)₂), 0.89 (m, 2H, CH(CH₂)₂), 2.47 (m, 1H, CH(CH₂)₂), 3.75 (s, 3H, OCH₃), 4.63 (s, 2H, 3-CH₂), 6.96 (s, 4H, 2'-H/3'-H/5'-H/6'-H), 6.99 (d, J = 2.9 Hz, 1H, 8-H), 7.20 (dd, J = 9.2, 2.9 Hz, 1H, 6-H), 7.32 (d, J = 9.2 Hz, 1H, 5-H), 7.94 (s, 1H, NH); ¹³C NMR (DMSO- d_6) δ 8.3 (CH(CH₂)₂), 29.8 (CH(CH₂)₂), 55.4 (OCH₃), 61.1 (C-3), 112.4 (C-8), 115.1 (C-3'/C-5'), 116.6 (C-5), 119.9 (C-2'/C-6'), 123.4 (C-8a), 123.9 (C-6), 140.2 (C-4a), 148.9 (C-7), 150.0 (C-4'), 154.5 (C-1'). Anal. (C₁₇H₁₈N₂O₄S) Calcd: C, 58.94; H, 5.24; N, 8.09; S, 9.25. Found: C, 59.27; H, 5.29; N, 8.20; S, 9.25.

4-Cyclopropyl-7-(3-cyanophenoxy)-3,4-dihydro-2H-1,2,4-benzothiadiazine 1,1-Dioxide (11b): 13% yield, mp 198–200 °C; ¹H NMR (DMSO-*d*₆) δ 0.68 (m, 2H, CH(CH₂)₂), 0.91 (m, 2H, CH(CH₂)₂), 2.52 (m, 1H, CH(CH₂)₂), 4.68 (s, 2H, 3-CH₂), 7.27 (m, 2H, 8-H/6'-H), 7.31 (dd, *J* = 9.1, 2.8 Hz, 1H, 6-H), 7.36 (d, *J* = 9.2 Hz, 1H, 5-H), 7.41 (d, *J* = 2.4 Hz, 1H, 2'-H), 7.57 (m, 2H, 4'-H/5'-H), 7.98 (bs, 1H, NH); ¹³C NMR (DMSO-*d*₆) δ 8.4 (CH(CH₂)₂), 29.8 (CH(CH₂)₂), 61.0 (C-3), 112.6 (C-3'), 115.3 (C-8), 116.8 (C-5), 118.2 (CN), 120.5 (C-2'), 122.2 (C-6'), 123.5 (C-8a), 125.6 (C-6), 126.8 (C-4'), 131.5 (C-5'), 141.5 (C-4a), 145.6 (C-7), 158.0 (C-1'). Anal. (C₁₇H₁₃N₃O₃S) Calcd: C, 59.81; H, 4.43; N, 12.31; S, 9.39. Found: C, 59.82; H, 4.71; N, 11.96; S, 8.66.

Stable Transfection of GluA2_o(Q) in HEK293 Cells. Human embryonic kidney 293 (HEK293) cells were transfected using the x-tremegene 9 3–1 kit (Sigma-Aldrich, St Louis, Missouri, USA). Briefly, an expression vector (a mixture of 2.5 μg of pcDNA3.1.Myc-GluA2_o(Q) and 7.5 μL of x-tremegene 9 in a buffer of optiMEM) was added on nearly confluent HEK293 cells in a 50 mm dish. A day later, the antibiotic G418 (700 μg/mL) was added to make the selection.

Fluorescence-Based Calcium Assay on GluA2(Q) Cells. HEK293 cells stably expressing AMPA tetrameric channel form A2 (Q) flop isoform (GluA2_o(Q)) were prepared. HEK293 cells or their stable cell line equivalents were routinely grown in Dulbecco's Modified Eagle's Medium (DMEM) containing 10% fetal bovine serum (FBS). The measurement of the fluorescence intensity was carried out using fluorescent microplate reader Fluoroskan Ascent FT equipped with two dispensers (Thermo Electron Corporation, Finland). After trypsinization, the cells were washed twice using Hanks balanced salt solution (HBS, 120 mM NaCl, 2 mM KCl, 2 mM CaCl₂, 2 mM MgCl₂, 10 mM HEPES, pH 7.4) and incubated for 1 h with fluorescent dye Fluo-4/AM (5 μg/mL; Molecular Probes, Invitrogen, Merelbeke Belgium). The cells were rinsed twice with HBS, and 100 μL of the resulting cell suspension in HBS buffer was introduced into each well of a 96-well plate (density of 150 000 cells/well). The evaluated compounds were applied at various concentrations (from 3 × 10⁻⁸ M to 10⁻⁴ M, with maximal DMSO concentration = 1%). After shaking the plate 30 s at 1200 rpm, the emission was read at 538 nm after an excitation at 485 nm during 500 ms per measure. Measurement of a vehicle control was followed by injection of a 10 mM glutamate solution (10 μL), a fluorescence measurement, 15 s of shaking at 1200 rpm and a final fluorescence measurement. The results (EC₅₀) are the concentration required to reach half of the maximal intensity, calculated by nonlinear regression analysis (GraphPad Prism software) from at least three independent concentration–response curves made in triplicate.

Expression and Purification. Rat GluA2-LBD, comprising segment S1 residues 413–527, a GT-linker, and segment S2 residues 653–807 (UNP P19491; numbering with signal peptide) as well as GluA2-LBD-L504Y–N775S were expressed and purified following the previously described procedure.³¹ For the SAXS experiments, the construct was identical except that the L504Y mutation was not present (GluA2-LBD-N775S).

Small-Angle X-ray Scattering. SAXS experiments were conducted as previously described.¹¹ Briefly, GluA2-LBD-N775S was concentrated to 3 mg/mL (0.1 mM) in SAXS buffer (10 mM glutamate, 25 mM NaCl, 25 mM Tris-Cl, pH 7) and subsequently diluted to the appropriate concentration (0.005–0.1 mM) with SAXS buffer. Loaded samples consisted of 1 μL of appropriately diluted modulator stock solubilized (in DMSO) and 29 μL of diluted protein. All SAXS experiments were collected at the Cornell High-Energy Synchrotron Source (CHESS)'s G1 beamline using a dual Pilatus 100 K–S SAXS/WAXS detector.^{32,33} Capillary cells were robotically loaded with the 30 μL precentrifuged samples, maintained at 4 °C, and thoroughly washed between samples.³⁴ For 0.005, 0.01, and 0.03 mM concentrations of **11m**, each sample condition and SAXS buffer was loaded and measured as three 30 μL replicates. The three scattering curves were averaged together for analysis. Background subtraction with matching buffer and data analysis were performed with RAW software.³⁵ The fraction of dimer was determined from

experimental SAXS data using the OLIGOMER program from the ATSAS suite.²⁴ Theoretical CRYSOLO-derived²⁴ form factors were based on monomeric and dimeric glutamate-bound GluA2-LBD-N775S structures.

Data were analyzed based on the equilibrium models in Figure 3A.¹¹ For the model with one site per dimer interface the degree of dimerization is given by

$$\bar{R} = \frac{-1 + \sqrt{1 + \left(\frac{8R_t}{K_4} \left(1 + \frac{M}{K_3}\right)\right)}}{1 + \sqrt{1 + \left(\frac{8R_t}{K_4} \left(1 + \frac{M}{K_3}\right)\right)}}$$

where *R_t* is the total GluA2-LBD-N775S concentration and *M* is the free modulator concentration. *K₄* and *K₃* are defined in Figure 3A. The degree of dimerization for two sites per dimer interface is given by

$$\bar{R} = \frac{-1 + \sqrt{1 + \left(\frac{8R_t}{K_4} \left(1 + \frac{2M}{K_3} + \frac{M^2}{K_3^2}\right)\right)}}{1 + \sqrt{1 + \left(\frac{8R_t}{K_4} \left(1 + \frac{2M}{K_3} + \frac{M^2}{K_3^2}\right)\right)}}$$

Since only the degree of dimerization is measured, there is no direct measure of the free modulator. In order to appropriately fit the data, the fitting routine generates a curve for values of *K₃* and *K₄* as a function of *M* and then calculates the total modulator at each point, generating a new curve for dimerization vs total modulator. In this way, the predicted results can be compared to the data. This is particularly important in cases in which the concentration of GluA2-LBD-N775S approaches that of the modulator (see **11m** in Figure 3B).

The value of *K₄* was fit simultaneously to all of the SAXS data, as this parameter was common to all modulators and all protein concentrations. As part of that global fit, the *K₃* was fit simultaneously to all data (i.e., data from all protein concentrations) for a given modulator. In that way, the *K₄* value was constrained by all of the data across all modulators and protein concentrations, and *K₃* was constrained by all of the data for a given modulator. This approach was used previously,¹¹ but in this case, the minimum for the *K₄* value was much better defined because of the additional data used in the fit.

Crystallization of GluA2-LBD-L504Y–N775S with 3. To GluA2-LBD-L504Y–N775S (4.5 mg/mL in 10 mM HEPES pH 7.0, 20 mM NaCl, 1 mM EDTA) were added glutamate to a final concentration of 1 mM and **3** as solid compound. The solution was equilibrated at 6 °C overnight prior to use. The protein–ligand complex was crystallized by the hanging-drop vapor-diffusion method at 6 °C. The reservoir volume was 500 μL and consisted of 18% PEG4000, 0.23 M lithium sulfate, and 0.1 M phosphate citrate, pH 4.5. Drops consisted of 1 μL of a protein solution mixed with 1 μL of the reservoir solution. Crystals were briefly submerged into the reservoir solution containing 20% glycerol as a cryo-protectant and flash cooled in liquid nitrogen before storage.

Crystallization of GluA2-LBD with 11m. To GluA2-LBD (5 mg/mL in 10 mM HEPES pH 7.0, 20 mM NaCl, 1 mM EDTA) were added glutamate to a final concentration of 5 mM and **11m** as solid compound due to the low solubility of the compound. The solution was equilibrated at 6 °C for 24 h prior to use. The protein–ligand complex was crystallized by the hanging-drop vapor-diffusion method at 6 °C. The reservoir volume was 500 μL and consisted of 15.2% PEG4000, 0.3 M zinc acetate, and 0.1 M sodium acetate, pH 5.5. Drops consisted of 1 μL of a protein solution mixed with 1 μL of the reservoir solution. Crystals were briefly submerged into reservoir solution containing 20% glycerol as a cryo-protectant and flash cooled in liquid nitrogen before storage.

Structure Determination. X-ray diffraction data were collected at beamline I911–3 at MAX-lab, Lund, Sweden³⁶ at a cryogenic temperature (100 K). The data were processed using XDS³⁷ and SCALA³⁸ in the CCP4 suite of programs.³⁹ The two structures were solved by molecular replacement in PHASER⁴⁰ using only the protein

atoms of the search model (PDB entry 3TKD (moA) for structure with **3** and PDB entry 3TDJ (moA) for structure with **11m**). Initial model building was performed using AUTOBUILD⁴¹ in PHENIX⁴² and water molecules were introduced into the structures at this step. During iterative rounds of model building and editing in COOT⁴³ and refinement in PHENIX, ligand molecules, other additives, and additional water molecules were gradually built into the structures. Coordinate files for **3** and **11m** were generated in MAESTRO (v.9.4; Schrödinger, LLC, New York, NY, 2013) and parameter files in eLBOW keeping the geometry.⁴⁴ The structures were refined using individual isotropic B values, TLS, NCS, and riding H atoms. The structures were validated by build-in tools in COOT, MolProbity⁴⁵ in PHENIX, and the wwPDB Validation Service. Domain closure of GluA2-LBD relative to the apo structure of GluA2-LBD (PDB entry 1FTO, moA) was calculated using the DynDom server.⁴⁶ Figures were prepared in PyMOL (v.1.7; The PyMOL Molecular Graphics System, V.S., LLC).

NMR Spectroscopy. GluA2-LBD-N775S was uniformly labeled with ¹⁵N and prepared for NMR spectroscopy as described previously.⁴⁷ Spectra were collected on a Bruker AVANCE III HD 800 MHz NMR spectrometer at the SUNY ESF NMR facility. A total of 1024 complex points were collected in the proton dimension (spectral width of 14423 Hz), and 128 complex increments were collected in the nitrogen dimension (spectral width of 3080 Hz). Data were analyzed with NMRPipe⁴⁸ and NMRFAM-SPARKY.⁴⁹ Figure 6B was prepared with Chimera.⁵⁰

■ ASSOCIATED CONTENT

📄 Supporting Information

The Supporting Information is available free of charge on the ACS Publications website at DOI: 10.1021/acs.jmedchem.7b01323.

Experimental SAXS data (PDF)

Molecular formula strings of the target compounds (CSV)

Accession Codes

The structure coordinates and corresponding structure factor file of GluA2-LBD-L483Y-N754S with glutamate and **3** have been deposited in the Protein Data Bank under the accession code 5O9A and the structure of GluA2-LBD with glutamate and **11m** with accession code 5OEW.

■ AUTHOR INFORMATION

Corresponding Authors

*E-mail: j.hanson@uliege.be (for pharmacological assays).

*E-mail: reo1@cornell.edu (for SAXS and protein NMR).

*E-mail: jsk@sund.ku.dk (for structure determination).

*E-mail: pierre.francotte@uliege.be (for synthetic and medicinal chemistry).

ORCID

Christopher P. Ptak: 0000-0003-2752-0367

Lars Olsen: 0000-0002-7607-7130

Jette Sandholm Kastrup: 0000-0003-2654-1510

Pierre Francotte: 0000-0001-9252-7798

Author Contributions

[†]E.G. and T.D. contributed equally.

Funding

J.H. and T.D. are a F.R.S.-FNRS research associate and Ph.D. fellow, respectively. P.G. is a Télévie Ph.D. fellow. This work was supported by the Fonds pour la Recherche Scientifique (F.R.S.-FNRS) Incentive Grant for Scientific Research [F.4510.14], Fonds Léon Frédéricq (Drapier, Gilissen), University of Liège [Fonds Spéciaux], Lundbeck Foundation (Larsen, Frydenvang, Kastrup), Danish Council for Independ-

ent Research (Laulumaa, Kastrup), Novo Nordisk Foundation (Kastrup), GluTarget (Larsen, Frydenvang, Kastrup), Danskatt (Larsen, Frydenvang, Rovinskaja, Kastrup), CoNeXT (Larsen, Kastrup), BioStruct-X (Frydenvang, Rovinskaja, Kastrup), and NIH (NS085239 and GM068935, Oswald). CHESS is supported by the NSF and NIH/NIGMS via the NSF award DMR-1332208, and the MacChess resource is supported by the NIGMS award GM-103485.

Notes

The authors declare no competing financial interest.

■ ACKNOWLEDGMENTS

Heidi Peterson is thanked for the help with expression and purification of the ligand-binding domain of GluA2. MAX-Lab, Lund, Sweden is thanked for providing beamtime.

■ ABBREVIATIONS USED

AMPA, AMPA receptor; ATD, amino-terminal domain; BDNF, brain-derived neurotrophic factor; BTZ, benzothiadiazine 1,1-dioxide; CTD, cytoplasmic terminal domain; GluA2-LBD, ligand-binding domain of GluA2; HFMZ, hydroflumethiazide; HSQC-TROSY, heteronuclear single quantum coherence transverse relaxation optimized spectroscopy; KA, kainic acid; SAXS, small-angle X-ray scattering; TMD, transmembrane domain

■ REFERENCES

- (1) Dingledine, R.; Borges, K.; Bowie, D.; Traynelis, S. F. The glutamate receptor ion channels. *Pharmacol. Rev.* **1999**, *51*, 7–61.
- (2) Traynelis, S. F.; Wollmuth, L. P.; McBain, C. J.; Menniti, F. S.; Vance, K. M.; Ogden, K. K.; Hansen, K. B.; Yuan, H.; Myers, S. J.; Dingledine, R. Glutamate receptor ion channels: structure, regulation, and function. *Pharmacol. Rev.* **2010**, *62*, 405–496.
- (3) Huganir, R. L.; Nicoll, R. A. AMPARs and synaptic plasticity: the last 25 years. *Neuron* **2013**, *80*, 704–717.
- (4) Lynch, G.; Palmer, L. C.; Gall, C. M. The likelihood of cognitive enhancement. *Pharmacol., Biochem. Behav.* **2011**, *99*, 116–129.
- (5) Partin, K. M. AMPA receptor potentiators: from drug design to cognitive enhancement. *Curr. Opin. Pharmacol.* **2015**, *20*, 46–53.
- (6) Jourdi, J.; Hsu, Y.-T.; Zhou, M.; Qin, Q.; Bi, X.; Baudry, M. Positive AMPA receptor modulation rapidly stimulates BDNF release and increases dendritic mRNA. *Transl. J. Neurosci.* **2009**, *29*, 8688–8697.
- (7) Clarkson, A. N.; Overman, J. J.; Zhong, S.; Mueller, R.; Lynch, G.; Carmichael, S. T. AMPA receptor-induced local brain-derived neurotrophic factor signaling mediates motor recovery after stroke. *J. Neurosci.* **2011**, *31*, 3766–3775.
- (8) Gan, Q.; Salussolia, C. L.; Wollmuth, L. P. Assembly of AMPA receptors: mechanisms and regulation. *J. Physiol.* **2015**, *593*, 39–48.
- (9) Sager, C.; Terhag, J.; Kott, S.; Hollmann, M. C-terminal domains of transmembrane α -amino-3-hydroxy-5-methyl-4-isoxazole propionate (AMPA) receptor regulatory proteins not only facilitate trafficking but are major modulators of AMPA receptor function. *J. Biol. Chem.* **2009**, *284*, 32413–32424.
- (10) Arai, A. C.; Kessler, M.; Rodgers, G.; Lynch, G. Effects of the Potent Ampakine CX614 on hippocampal and recombinant AMPA receptors: interactions with cyclothiazide and GYKI 52466. *Mol. Pharm.* **2000**, *58*, 802–813.
- (11) Ptak, C. P.; Hsieh, C. L.; Weiland, G. A.; Oswald, R. E. Role of stoichiometry in the dimer-stabilizing effect of ampa receptor allosteric modulators. *ACS Chem. Biol.* **2014**, *9*, 128–133.
- (12) Ptak, C. P.; Ahmed, A. H.; Oswald, R. E. Probing the allosteric modulator binding site of GluR2 with thiazide derivatives. *Biochemistry* **2009**, *36*, 8594–8602.

- (13) Pirotte, B.; Francotte, P.; Goffin, E.; de Tullio, P. AMPA receptor positive allosteric modulators: a patent review. *Expert Opin. Ther. Pat.* **2013**, *23*, 615–628.
- (14) Citti, C.; Battisti, U. M.; Cannazza, G.; Jozwiak, K.; Stasiak, N.; Puja, G.; Ravazzini, F.; Ciccarella, G.; Braghiroli, D.; Parenti, C.; Troisi, L.; Zoli, M. 7-Chloro-5-(furan-3-yl)-3-methyl-4H-benzo[e][1,2,4]-thiadiazine 1,1-dioxide as positive allosteric modulator of α -amino-3-hydroxy-5-methyl-4-isoxazolepropionic acid (AMPA) receptor. the end of the unsaturated-inactive paradigm? *ACS Chem. Neurosci.* **2016**, *7*, 149–160.
- (15) Battisti, U. M.; Citti, C.; Rastelli, G.; Pinzi, L.; Puja, G.; Ravazzini, F.; Ciccarella, G.; Braghiroli, D.; Cannazza, G. An unexpected reversal in the pharmacological stereoselectivity of benzothiadiazine AMPA positive allosteric modulators. *MedChemComm* **2016**, *7*, 2410–2417.
- (16) Krintel, C.; Francotte, P.; Pickering, D. S.; Juknaitė, L.; Pøhlsgaard, J.; Olsen, L.; Frydenvang, K.; Goffin, E.; Pirotte, B.; Kastrup, J. S. Enthalpy-entropy compensation in the binding of modulators at ionotropic glutamate receptor GluA2. *Biophys. J.* **2016**, *110*, 2397–2406.
- (17) Larsen, A. P.; Francotte, P.; Frydenvang, K.; Tapken, D.; Goffin, E.; Fraikin, P.; Caignard, D. H.; Lestage, P.; Danober, L.; Pirotte, B.; Kastrup, J. S. Synthesis and pharmacology of mono-, di-, and trialkyl-substituted 7-chloro-3,4-dihydro-2H-1,2,4-benzothiadiazine 1,1-dioxides combined with x-ray structure analysis to understand the unexpected structure-activity relationship at AMPA receptors. *ACS Chem. Neurosci.* **2016**, *7*, 378–390.
- (18) Cordi, A.; Desos, P.; Lestage, P. N. *Benzothia(dia)zine derivatives and their use as ampa modulators*. U.S. Patent WO03053947 (A1), 2003.
- (19) Francotte, P.; de Tullio, P.; Goffin, E.; Dintilhac, G.; Graindorge, E.; Fraikin, P.; Lestage, P.; Danober, L.; Thomas, J.-Y.; Caignard, D.-H.; Pirotte, B. Design, synthesis, and pharmacology of novel 7-substituted 3,4-dihydro-2H-1,2,4-benzothiadiazine 1,1-dioxides as positive allosteric modulators of AMPA receptors. *J. Med. Chem.* **2007**, *50*, 3153–3157.
- (20) Nørholm, A. B.; Francotte, P.; Goffin, E.; Botez, I.; Danober, L.; Lestage, P.; Pirotte, B.; Kastrup, J. S.; Olsen, L.; Oostenbrink, C. Thermodynamic characterization of new positive allosteric modulators binding to the glutamate receptor A2 ligand-binding domain: combining experimental and computational methods unravels differences in driving forces. *J. Chem. Inf. Model.* **2014**, *54*, 3404–3416.
- (21) Francotte, P.; Nørholm, A. B.; Deva, T.; Olsen, L.; Frydenvang, K.; Goffin, E.; Fraikin, P.; de Tullio, P.; Challal, S.; Thomas, J. Y.; Iop, F.; Louis, C.; Botez-Pop, I.; Lestage, P.; Danober, L.; Kastrup, J. S.; Pirotte, B. positive allosteric modulators of 2-amino-3-(3-hydroxy-5-methylisoxazol-4-yl)propionic acid receptors belonging to 4-cyclopropyl-3,4-dihydro-2H-1,2,4-pyridothiadiazine dioxides and diversely chloro-substituted 4-cyclopropyl-3,4-dihydro-2H-1,2,4-benzothiadiazine 1,1-dioxides. *J. Med. Chem.* **2014**, *57*, 9539–9553.
- (22) Weiss, J. N. The Hill equation revisited: uses and misuses. *FASEB J.* **1997**, *11*, 835–841.
- (23) Nørholm, A. B.; Francotte, P.; Olsen, L.; Krintel, C.; Frydenvang, K.; Goffin, E.; Challal, S.; Danober, L.; Botez-Pop, I.; Lestage, P.; Pirotte, B.; Kastrup, J. S. Synthesis, pharmacological and structural characterization, and thermodynamic aspects of GluA2-positive allosteric modulators with a 3,4-dihydro-2H-1,2,4-benzothiadiazine 1,1-dioxide scaffold. *J. Med. Chem.* **2013**, *56*, 8736–8745.
- (24) Petoukhov, M. V.; Franke, D.; Shkumatov, A. V.; Tria, G.; Kikhney, A. G.; Gajda, M.; Gorba, C.; Mertens, H. D.; Konarev, P. V.; Svergun, D. I. New developments in the ATSAS program package for small-angle scattering data analysis. *J. Appl. Crystallogr.* **2012**, *45*, 342–350.
- (25) Sun, Y.; Olson, R.; Horning, M.; Armstrong, N.; Mayer, M.; Gouaux, E. Mechanism of glutamate receptor desensitization. *Nature* **2002**, *417*, 245–253.
- (26) Ahmed, A. H.; Ptak, C. P.; Oswald, R. E. Molecular mechanism of flop selectivity and subsite recognition for an AMPA receptor allosteric modulator: structures of GluA2 and GluA3 in complexes with PEPA. *Biochemistry* **2010**, *49*, 2843–2850.
- (27) Dunitz, J. D.; Taylor, R. Organic Fluorine hardly ever accepts hydrogen bonds. *Chem. - Eur. J.* **1997**, *3*, 89–98.
- (28) Francotte, P.; Goffin, E.; Fraikin, P.; Lestage, P.; Van Heugen, J.-C.; Gillotin, F.; Danober, L.; Thomas, J.-Y.; Chiap, P.; Caignard, D.-H.; Pirotte, B.; De Tullio, P. New fluorinated 1,2,4-benzothiadiazine 1,1-dioxides: discovery of an orally active cognitive enhancer acting through potentiation of the 2-amino-3-(3-hydroxy-5-methylisoxazol-4-yl)propionic acid receptors. *J. Med. Chem.* **2010**, *53*, 1700–1711.
- (29) Clark, T.; Hennemann, M.; Murray, J. S.; Politzer, P. Halogen bonding: the σ -hole. *J. Mol. Model.* **2007**, *13*, 291–296.
- (30) Politzer, P.; Murray, J. S.; Clark, T. Halogen bonding: an electrostatically-driven highly directional noncovalent interaction. *Phys. Chem. Chem. Phys.* **2010**, *12*, 7748–7757.
- (31) Krintel, C.; Frydenvang, K.; Olsen, L.; Kristensen, M. T.; de Barrios, O.; Naur, P.; Francotte, P.; Pirotte, B.; Gajhede, M.; Kastrup, J. S. Thermodynamics and structural analysis of positive allosteric modulation of the ionotropic glutamate receptor GluA2. *Biochem. J.* **2012**, *441*, 173–178.
- (32) Skou, S.; Gillilan, R. E.; Ando, N. Synchrotron-based small-angle X-ray scattering of proteins in solution. *Nat. Protoc.* **2014**, *9*, 1727–1739.
- (33) Acerbo, A. S.; Cook, M. J.; Gillilan, R. E. Upgrade of MacCHESS facility for X-ray scattering of biological macromolecules in solution. *J. Synchrotron Radiat.* **2015**, *22*, 180–186.
- (34) Nielsen, S. S.; Møller, M.; Gillilan, R. E. High-throughput biological small-angle X-ray scattering with a robotically loaded capillary cell. *J. Appl. Crystallogr.* **2012**, *45*, 213–223.
- (35) Hopkins, J. B.; Gillilan, R. E.; Skou, S. BioXTAS RAW: improvements to a free open-source program for small-angle X-ray scattering data reduction and analysis. *J. Appl. Crystallogr.* **2017**, *50*, 1545–1553.
- (36) Ursby, T.; Unge, J.; Appio, R.; Logan, D. T.; Fredslund, F.; Svensson, C.; Larsson, K.; Labrador, A.; Thunnissen, M. M. G. M. The macromolecular crystallography beamline I911–3 at the MAX IV laboratory. *J. Synchrotron Radiat.* **2013**, *20*, 648–653.
- (37) Kabsch, W. XDS. *Acta Crystallogr., Sect. D: Biol. Crystallogr.* **2010**, *66*, 125–132.
- (38) Evans, P. Scaling and assessment of data quality. *Acta Crystallogr., Sect. D: Biol. Crystallogr.* **2006**, *62*, 72–82.
- (39) Winn, M. D.; Ballard, C. C.; Cowtan, K. D.; Dodson, E. J.; Emsley, P.; Evans, P. R.; Keegan, R. M.; Krissinel, E. B.; Leslie, A. G. W.; McCoy, A.; McNicholas, S. J.; Murshudov, G. N.; Pannu, N. S.; Potterton, E. A.; Powell, H. R.; Read, R. J.; Vagin, A.; Wilson, K. S. Overview of the CCP4 suite and current developments. *Acta Crystallogr., Sect. D: Biol. Crystallogr.* **2011**, *67*, 235–242.
- (40) McCoy, A. J.; Grosse-Kunstleve, R. W.; Adams, P. D.; Winn, M. D.; Storoni, L. C.; Read, R. J. Phaser crystallographic software. *J. Appl. Crystallogr.* **2007**, *40*, 658–674.
- (41) Terwilliger, T. C.; Grosse-Kunstleve, R. W.; Afonine, P. V.; Moriarty, N. W.; Zwart, P. H.; Hung, L. W.; Read, R. J.; Adams, P. D. Iterative model building, structure refinement and density modification with the PHENIX AutoBuild wizard. *Acta Crystallogr., Sect. D: Biol. Crystallogr.* **2008**, *64*, 61–69.
- (42) Adams, P. D.; Afonine, P. V.; Bunkóczi, G.; Chen, V. B.; Davis, I. W.; Echols, N.; Headd, J. J.; Hung, L. W.; Kapral, G. J.; Grosse-Kunstleve, R. W.; McCoy, A. J.; Moriarty, N. W.; Oeffner, R.; Read, R. J.; Richardson, D. C.; Richardson, J. S.; Terwilliger, T. C.; Zwart, P. H. PHENIX: a comprehensive Python-based system for macromolecular structure solution. *Acta Crystallogr., Sect. D: Biol. Crystallogr.* **2010**, *66*, 213–221.
- (43) Emsley, P.; Lohkamp, B.; Scott, W. G.; Cowtan, K. Features and development of Coot. *Acta Crystallogr., Sect. D: Biol. Crystallogr.* **2010**, *66*, 486–501.
- (44) Moriarty, N. W.; Grosse-Kunstleve, R. W.; Adams, P. D. electronic Ligand Builder and Optimization Workbench (eLBOW): a tool for ligand coordinate and restraint generation. *Acta Crystallogr., Sect. D: Biol. Crystallogr.* **2009**, *65*, 1074–1080.

(45) Chen, V. B.; Arendall, W. B.; Headd, J. J.; Keedy, D. A.; Immormino, R. M.; Kapral, G. J.; Murray, L. W.; Richardson, J. S.; Richardson, D. C. *MolProbity*: all-atom structure validation for macromolecular crystallography. *Acta Crystallogr., Sect. D: Biol. Crystallogr.* **2010**, *66*, 12–21.

(46) Hayward, S.; Berendsen, H. J. C. Systematic analysis of domain motions in proteins from conformational change; new results on citrate synthase and T4 lysozyme. *Proteins: Struct., Funct., Genet.* **1998**, *30*, 144–154.

(47) Ptak, C. P.; Ahmed, A. H.; Oswald, R. E. NMR approaches to functional dynamics of genetically separated iGluR domains. *Neuro-methods* **2016**, *106*, 101–118.

(48) Delaglio, F.; Grzesiek, S.; Vuister, G. W.; Zhu, G.; Pfeifer, J.; Bax, A. NMRPipe: a multidimensional spectral processing system based on UNIX pipes. *J. Biomol. NMR* **1995**, *6*, 277–293.

(49) Lee, W.; Tonelli, M.; Markley, J. L. NMRFAM-SPARKY: enhanced software for biomolecular NMR spectroscopy. *Bioinformatics* **2015**, *31*, 1325–1327.

(50) Pettersen, E. F.; Goddard, T. D.; Huang, C. C.; Couch, G. S.; Greenblatt, D. M.; Meng, E. C.; Ferrin, T. E. UCSF Chimera—a visualization system for exploratory research and analysis. *J. Comput. Chem.* **2004**, *25*, 1605–1612.